1 **Title: NBR1 -mediated selective autophagy of ARF7 modulates root branching**

2 **Running title: Autophagy modulates root branching**

3 Ebstrup E[1+], Ansbøl J[1+], Chevalier J[1],Clemmens P[1], Rodriguez E[1*]

4 [1]Innate immunity and cellular reprogramming group. Functional Genomic section, Department of
5 Biology, University of Copenhagen, Denmark.

6 [+]These authors contributed equally to this work.

7 *Correspondence to: Eleazar.rodriguez@bio.ku.dk

8

Abstract

Auxin orchestrates growth and developmental regulation in plants. For instance, auxin dictates root architecture via the Auxin Response Factor (ARF) family of transcription factors, which control lateral root (LR) formation. In *Arabidopsis*, ARF7 is essential for the correct definition of LR's prebranch sites (PBS) through gene expression oscillation and plays a pivotal role during LR initiation. Despite ARF7's importance to this process, there is a surprising lack of knowledge about how ARF7's turnover is regulated and how this contributes to root architecture patterning. Here, we show that ARF7 accumulates in autophagy mutants and is degraded through NBR1-dependent selective autophagy. Moreover, our data indicates that the previously reported rhythmic changes to ARF7 abundance in the root's oscillation zone its observed in the rest of the plant and this is modulated via autophagy. Surprisingly, autophagy deficiency did not seem to cause major changes in PBS establishment but ultimately reduces LR formation. In support of these findings, our microscopy data shows that ARF7 and autophagy markers mainly co-localize in mature tissue and the process can be triggered by auxin. In conclusion we report a novel role for autophagy during plant development, namely by enacting auxin-induced selective degradation of ARF7 to optimize root branching.

Introduction

The plant root system plays a fundamental role as a point of contact with the plant's surroundings and allows adaptation to multiple stresses. Contrary to primary roots, lateral root (LR) development is post embryonic, which means that LR architecture is heavily influenced by growth conditions (Lv *et al*, 2021). As LR growth is modular, perception of the correct developmental conditions authorizes the repetition of LR modules along the primary root, maximizing the root's surface area. LRs originate from a cell layer called pericycle which surrounds the vasculature, and occurs sequentially in 4 steps: positioning, initiation, outgrowth, and emergence. During the positioning step, the plant ensures the spatiotemporal distribution, priming and activation of LR founder cells (LRFC) (Du & Scheres, 2018). LR spacing is controlled by an oscillatory root clock which dictates gene expression and cycles every 4-6 hours (Moreno-Risueño *et al*, 2010; Wachsman *et al*, 2020). This oscillatory clock is regulated, among others, by the phytohormone auxin and can be characterized through monitoring of reporter markers under the control of DR5, a synthetic promoter containing tandem repeats of an auxin responsive TGTCTC element (Ulmasov *et al*, 1997). DR5 expression analyses lead to definition of 2 contrasting oscillation phases: in-phase (concurrent with DR5 maximum signal) and anti-phase (DR5 minimum signal) which reciprocally repress each other (Moreno-Risueño *et al*, 2010). One of the genes displaying anti-phase expression is AUXIN RESPONSIVE FACTOR 7 (*ARF7*), a key transcription factor (TF) which, among others, regulates LR formation (Okushima *et al*, 2007). Importantly, analysis of *ARF7* loss of function mutant (Moreno-Risueño *et al*, 2010; Perianez-Rodriguez *et al*, 2021) indicates that this TF's oscillation is essential for the correct establishment of LR prebranch sites (PBS).

While positioning and initiation are broadly regulated by different mechanisms, ARF7 and its 2 direct targets LATERAL ORGAN BOUNDARIES DOMAIN (LBD) 16 and LBD33 are among the few genes that participate in both processes (Moreno-Risueño *et al*, 2010); this attests to ARF7's pivotal role in organizing root architecture. During the initiation step, the auxin signalling node IAA14-ARF7-ARF19 controls LBD16 activation in the LRFC, which is necessary to achieve asymmetry and initiate cell division (Goh *et al*, 2019). In addition to the importance of *ARF7* transcriptional oscillation for LR formation, it has also been shown that the subcellular localization of ARF7 is important for its function: nuclear localization correlates with auxin responsive tissue while in less responsive areas, activating ARFs concentrate to form cytoplasmic condensates with liquid-like and solid-like proprieties (Powers *et al*, 2019). These body of evidence demonstrate the regulatory complexity coordinating ARFs-dependent responses, as an intricate web of processes tightly regulate ARFs levels and compartmentalization. Yet surprisingly, little is known about how ARF7 proteostasis is managed and how it impacts the cellular decision making behind LR formation authorization.

59 Macroautophagy (herein autophagy) is an evolutionary conserved catabolic process which partakes
60 in cellular recycling of macromolecules and organelles (Levine & Klionsky, 2004). Autophagy is
61 characterized by the formation of an isolation membrane enclosing a portion of cytoplasm to form a
62 double-membraned vesicle termed the autophagosome. Originally characterized during starvation
63 stress, autophagy was viewed as a random process due to the observation of what seemed to be an
64 indiscriminate engulfment of portions of the cytoplasm. Further studies unveiled the existence of
65 several selective cargo adaptors which allow for targeted degradation of cellular constituents (*e.g.,*
66 (Svenning *et al*, 2011; Nolan *et al*, 2017; Stephani *et al*, 2020; Wu *et al*, 2021), meaning that
67 autophagy can be highly selective and participate in targeted remodelling of the cell. Perhaps one of
68 the most characterized cargo receptors in plants is NEIGHBOUR OF BRCA1 (NBR1, Svenning *et al*,
69 2011), a hybrid of mammalian *NBR1* and *p62*, possessing a PB1 domain necessary for
70 homopolymerization and biomolecular condensate formation, and an UBA domain for ubiquitin
71 binding. It is through the latter that NBR1 binds ubiquitinated cargo, which are then targeted for
72 autophagic degradation via NBR1's interaction with the autophagosome decorating proteins ATG8s
73 (*e.g.,* Zhou et al, 2013, 2014; Hafrén et al, 2017; Ji et al, 2020; Tarnowski et al, 2020). The ability to
74 function selectively allows autophagy to participate in a variety of stress responses, namely by
75 promoting the cellular reprogramming necessary to enact appropriated responses (Rodriguez *et al*,
76 2020). Without surprise, autophagic deficiency has been shown to cause myriads of developmental
77 defects; interference with core autophagic machinery component often causes lethality during early
78 developmental stages, severe developmental defects, and shortened life span in metazoans (*e.g.,*
79 Scott *et al*, 2004; Liu *et al*, 2015; Yoshii *et al*, 2016). In contrast, plants are able to tolerate disruption
80 of autophagy activity without major penalties: autophagy deficient mutants display subtle growth
81 phenotypes like reduced biomass, inflorescence numbers and premature senescence (Bassham *et al*,
82 2006), but importantly, are able to complete their life cycle and generate fertile progeny. It thus
83 seems that the phenotypic "struggles" of plant *atg* mutants become more apparent under stress, as
84 can be attested by the many publications linking autophagy with stress responses (Liu *et al*, 2009;
85 Hofius *et al*, 2009; Vanhee *et al*, 2011; Zhou *et al*, 2013b; Munch *et al*, 2014; Chen *et al*, 2015; Nolan
86 *et al*, 2017; Sedaghatmehr *et al*, 2019; Rodriguez *et al*, 2020). For instance, autophagy has been
87 shown to be involved in primary root growth and LR formation during nutrient starvation (Deb *et al*,
88 2014; Huang *et al*, 2019), which is consistent with the cross-kingdom descriptions of the starvation-
89 alleviating properties of autophagy (Scott *et al*, 2004; Desideri *et al*, 2012; Huang *et al*, 2015; Wu *et*
90 *al*, 2021). In contrast, the role of autophagy in regulating root architecture under normal
91 developmental conditions is less understood.

92 In this work, we explored the contribution of autophagy in mediating ARF7's dependent responses.
93 By using a combination of cell imaging, biochemical, genetics, molecular biology and proteomics
94 approaches, we demonstrate that ARF7's turnover is processed via NBR1-mediated selective
95 autophagy. Importantly, we demonstrate that ARF7's abundance rhythmically oscillates in the whole
96 plant and autophagy is necessary for proper establishment of ARF7's rhythm. Surprisingly, our data
97 indicates that autophagy mutants display normal PBS establishment but have reduced LR formation,
98 and together with ARF7 and ATG8 co-localization experiments, suggest that ARF7 might be regulated
99 by different mechanisms in a tissue specific manner. Additively, we show that short auxin treatment
100 is sufficient to trigger ARF7 to localize into cytoplasmic foci, regardless of the root zone, co-
101 localization of these cytoplasmic foci with ATG8a mainly occurs in the maturation zone. With these
102 findings, we reveal an important regulatory role for selective autophagy during auxin responses
103 through the turnover of the crucial auxin signalling regulator ARF7 and consequent fine-tuning of
104 root architecture.

105

106 **Results**

107 *Autophagy modulates* ARFs *turnover*

108 We have recently reported that autophagy participates in stem cell reprogramming and
109 differentiation in the distantly related species *P. patens* and *A. thaliana* (Rodriguez *et al*, 2020; Kanne
110 *et al*, 2021). Because *Arabidopsis* stem cell formation executes a program similar to LR formation
111 (Sugimoto *et al*, 2010), we wondered if key regulators of these processes might be modulated via
112 autophagy. As seen in Fig 1, ARF7 accumulates in different autophagy mutants and in the KO of the
113 autophagic cargo adaptor NBR1 (Fig 1A), when compared to Col-0. To address if the proteasome also
114 contributes to ARF7 proteostasis, we treated seedlings of those genotypes with the proteasome
115 inhibitor MG132 (Fig 1A). Col-0 samples treated with MG132 showed ARF7 accumulation to levels
116 comparable with those of untreated *atg* mutants. Moreover, simultaneous inhibition of both
117 degradation pathways leads to further accumulation of ARF7 which indicate that ARF7 proteostasis
118 is dependent on autophagy and the proteasome and it's in agreement with data by (Jing *et al*, 2022)
119 showing proteasomal degradation of ARF7. To rule out that elevated transcript levels in *atg* mutants
120 could be behind ARF7 accumulation in those lines, we performed qPCR and observed that *ARF7*'s
121 relative expression was around 30% lower in *atg* mutants than Col-0 (Fig 1B).

122 To further our claim that autophagy modulates ARF7 turnover, we introduced the translational
123 reporter *pARF7::gARF7-Venus* herein called *ARF7-Venus* (Orosa-Puente *et al*, 2018) into *atg2-1*

124 background. We then quantified ARF7-Venus levels by western blot analyses of protein extracts
125 from *ARF7-Venus* and *ARF7-Venus x atg2-1*¸ with this showing significantly higher levels of ARF7-
126 Venus when autophagy is dysfunctional (Fig 1C). Using the same lines, we also analysed ARF7-Venus
127 subcellular fluorescence intensity in the root's meristematic and maturation zones by confocal
128 microscopy (Fig 1 D-I). In agreement with our western blots, we detected significantly higher ARF7-
129 Venus fluorescence intensity in the *atg2-1* background for all tissues and subcellular localization
130 except for the meristem's nuclei (Fig1 I). Because ARF7 often works together with ARF19 during
131 regulation of root architecture, we also enquired about autophagy's role during ARF19 turnover.
132 Western blot probing of *pARF19::ARF19-GFP/nph4-1 arf19-1* seedlings (Okushima *et al*, 2007)
133 treated with or without the vacuolar protease inhibitors Pepstatin A and E-64D for 24h revealed
134 substantial accumulation of ARF19-GFP when vacuolar proteases were inhibited(Fig EV1) . Together,
135 our results indicate that autophagy participates in the turnover of these essential LR formation
136 regulators.

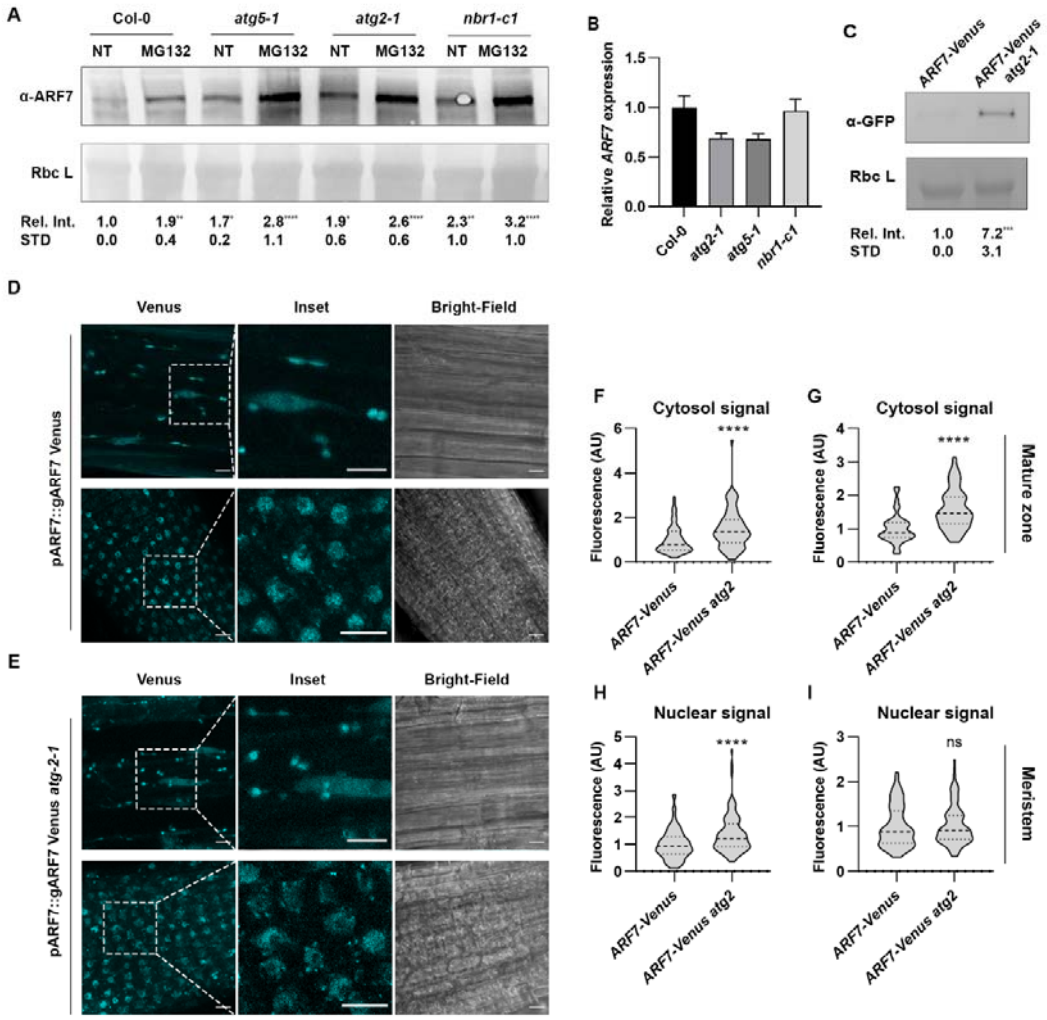

Figure 1*:* ARF7 is degraded via autophagy. **A**) ARF7 western blots of protein extracts from Col-0, *atg5-1*, *atg2-1* and *nbr1-c1* with or without addition of the proteasome inhibitor MG132. **B**) *ARF7* relative expression in given genotypes. *ARF7* expression was normalized to *ACTIN2* and is normalized to Col-0 (set to 1). The experiment was repeated 3 times (biological replicates) with similar results. **C**) GFP western blot of protein extracts from Col-0 or *atg2-1* expressing *ARF7-Venus*. Values below each band represent the relative intensity ratio between ARF7 (**A**) or ARF7-Venus (**C**) and RuBisCO large subunit (Rbc L) as stained with Ponceau S used as loading control. Ratios were normalized to untreated Col-0 NT (MS+ solvent) which was arbitrarily set to 1. Values provided are the average and SD of 5 **(A)** or 7 **(C)** biological replicates, asterisk depict statistical significance from Col-0 NT according to a Holm-Sidak test **(A)** or two-tailed t-test **(C)** (* 0.05; ** 0.01; **** 0.0001). **D-E**) Confocal images of root maturation zone (top panel) and meristematic zone (bottom panel) in Col-0 (**D**) or *atg2-1* (**E**) expressing *ARF7-Venus*. (**F-I**) Fluorescence intensity quantification of ARF7-Venus subcellular localization in given lines. The values presented for ARF7-Venus fluorescence intensity in *atg2-1* background in the maturation zone (**F-G**) or meristematic zone (**H-I**) were normalized to the values in Col-0 background (which was set to 1). The outline of the violin plots represents the probability of the kernel density. Dotted lines represent interquartile ranges (IQR), with the thick horizontal line representing the median; whiskers extend to the highest and lowest data point. Results were obtained from three independent experiments with at least 11 plants per condition being analysed in total. At least

153 40 nuclei and cytoplasmic regions were measured per genotype/tissue. Asterisks mark statistical significance to NT
154 according to a Mann-Whitney U-test (****P < 0.0001).

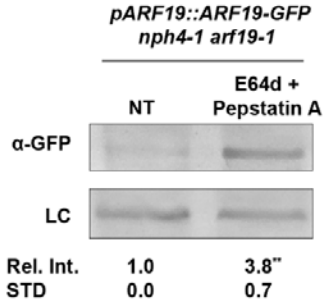

155

156 **Fig EV1**: Autophagy inhibition promotes ARF19 accumulation. GFP western blot of 14-day-old *pARF19::ARF19-GFP/nph4-1*
157 *arf19-1* seedlings grown in MS or MS supplemented with vacuolar protease inhibitors E-64D and Pepstatin A for 24h.
158 Values below each band represent the ratio between ARF19-GFP and the loading control (LC) normalized to NT (MS+
159 solvent), which was set to 1. Image is representative of 3 biological replicates; asterisk depict statistical significance from
160 NT according to a Man—Whitney U-test (P≤0.01)

161

162 ARF7 *interacts with* NBR1 *and* ATG8a *in planta*

163 To further substantiate our claim that autophagy participates in the targeted degradation of ARF7
164 we performed protein-protein interaction studies. For this purpose, we used *Arabidopsis* stable
165 transgenic lines expressing ARF7-Venus and performed coimmunoprecipitation (Co-IP) experiments.
166 The experiment revealed that NBR1 (Fig 2A) but not GOT1-YFP, co-immunoprecipitated with ARF7-
167 Venus; this is supported by ATG8a's enrichment in the same conditions (Fig 2B). Moreover, a web-
168 based analysis (Jacomin *et al*, 2016) identified several potential ATG8-interaction motifs (AIM) in
169 ARF7, supporting our findings. As a cautionary note, we were unable to detect ARF7-Venus in the
170 input of both Co-IPs which can likely be explained by the fact that ARF7-Venus is under the control of
171 its native promoter and thus lowly expressed. We also performed multi-colour Bimolecular
172 fluorescence complementation (mcBiFC) analysis with a system allowing simultaneous interaction
173 studies of several proteins (Gehl *et al*, 2009) to transiently express Venus^{N}-ARF7 with SCFP^{N}-ATG8a
174 and either SCFP^{C}-NBR1 or SCFP^{C}-TSPO, (TRYPTOPHAN-RICH SENSORY PROTEIN, an autophagic cargo
175 adaptor for aquaporins, Hachez *et al*, 2014) in *Nicotiana benthamiana* leaves. As expected, SCFP^{C}-
176 NBR1 and SCFP^{N}-ATG8a were able to reconstitute CFP to produce distinct fluorescence signal
177 localized in the nuclei and cytoplasm (Fig 2C). Moreover, Venus^{N}-ARF7 and SCFP^{C}-NBR1 produced
178 GFP signal, which was localized to the cytoplasm and nuclei, in many instances co-localizing with
179 NBR1-ATG8a CFP signal (Fig 2C). In contrast, SCFP^{C}-TSPO did not produce GFP signal when co-
180 expressed with Venus^{N}-ARF7. In combination, these results indicate that ARF7 interacts with

181 autophagic components and cumulative with data from Fig 1, indicate that this TF is degraded via
182 NBR1-mediated selective autophagy.

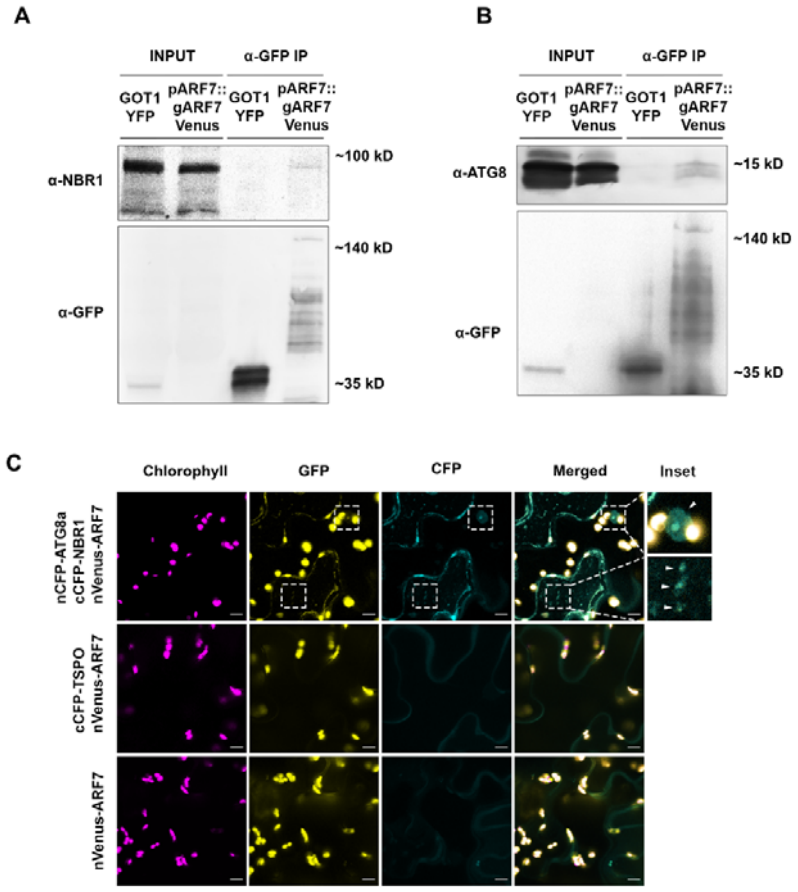

183

184 **Figure 2** ARF7 associates with autophagic components NBR1 and ATG8a. **A, B)** ARF7 and ATG8/NBR1 association was
185 tested by Coimmunoprecipitation (Co-IP) assay. Protein extracted from *Arabidopsis* lines expressing *pARF7::gARF7-Venus*
186 or free *YFP* were immunoprecipitated with anti-GFP antibody and subsequently probed with antibodies raised against
187 NBR1 or ATG8a. **C**) Bimolecular fluorescence complementation experiments shows oligomerization of ARF7, NBR1 and
188 ATG8a in *N. Benthamiana*. Images were taken 48 hpi. cCFP-TSPO was used as control. Insets display close-ups of examples
189 of reconstitution of GFP and CFP signal, which are also indicated by arrows. Etched boxes in GFP and CFP channels indicate
190 the place of the insets in those channels. Scale bar: 10 µM

191

192 *ARF7 co-localization with autophagosomes follows a daily rhythm and is triggered by auxin.*

193 Having established that autophagy regulates ARF7 abundance, it would be expected that this TF co-
194 localize with autophagosome-like structures. To assess this, we crossed ARF7-Venus to mCherry-
195 ATG8a and mCherry-NBR1 reporter lines (Svenning *et al*, 2011) and used this for live cell imaging. As
196 expected, both autophagy-related proteins localized to cytoplasmic foci, in many instances co-
197 localizing with ARF7-Venus (Fig 3A). Moreover, mCherry-ATG8a also co-localized with ARF7-Venus in

198 the nucleus (Fig 3A). It should be noted that the co-localization of these autophagic proteins with
199 ARF7 in cytoplasmic foci is mainly observable in the root's maturation zone; in younger tissue ARF7
200 primarily localizes in the nucleus but some instances of cytoplasmic co-localization are also
201 observable (Fig 3A & B). Our data is in agreement with previous reports demonstrating that ARF7
202 partitioning is dependent on developmental stage of the tissue (Orosa-Puente *et al*, 2018; Powers *et*
203 *al*, 2019).

204 ARF7's nucleo-cytopartitioning has been ascribed to liquid-liquid phase separation (LLPS) (Powers *et*
205 *al*, 2019); likewise, autophagosome formation sites and protein cargo triage (Kirkin *et al*, 2009;
206 Zhang *et al*, 2009; Fujioka *et al*, 2020) are also dependent on LLPS. To address the nature of these
207 cytoplasmic ARF7 & ATG8 foci, we incubated seedlings expressing mCherry-ATG8 and ARF7-Venus
208 with the LLPS inhibitor 1,6-hexanediol (Wang *et al*, 2021; Xie *et al*, 2021) and tracked the stability of
209 those foci over time. Most of the foci in which ARF7-Venus and mCherry-ATG8a co-localized were
210 sensitive to 1,6-hexanediol treatment (Fig EV2), suggesting that these structures have liquid-like
211 properties. Interestingly, some of these co-localizing events were insensitive to 1,6-hexanediol
212 treatment, even after prolonged exposure (*i.e.,* more than 30 min), indicating that those assembles
213 have solid-like properties. Our data is both in agreement with findings for ARF7 (Powers *et al*, 2019)
214 and studies in mammalians showing that NBR1 (and p62) is involved in condensate formation during
215 autophagic degradation of substrates (Turco *et al*, 2021).

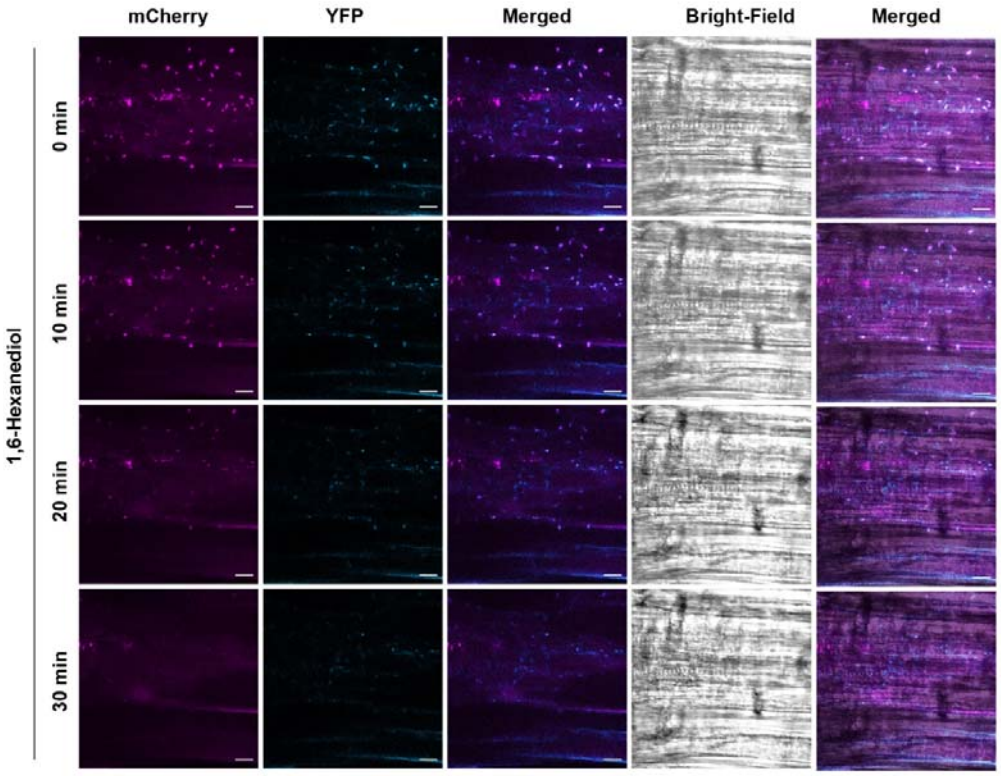

216

217 **Figure EV2** ARF7 and ATG8 condensates have both liquid and solid properties. *pARF7::gARF7-Venus* x *mCherry ATG8a*
218 plants were treated with the LLPS inhibitor 1,6-Hexanediol and imaged at given time points. Representative pictures were
219 taken in the maturation zone of 10–14-day old *Arabidopsis* seedlings. Leftmost Merge column represent the merger of YFP
220 and mCherry channels, while the rightmost also includes the T-PMT channel (Brightfield). Scale bar 10 µM.

221

222 While our data demonstrates that autophagy plays a clear role in controlling ARF7's abundance, the
223 factors/conditions leading to ARF7 turnover are unclear. To tackle this, we decided to treat *ARF7 -*
224 *Venus x mCherry ATG8a* seedlings with auxin or cytokinin treatment; our rationale being two-fold: a)
225 auxin (NAA) and cytokinin (Kinetin) often act in contrast to each other during many developmental
226 processes (Du & Scheres, 2018); b) we have recently shown that plants rapidly engage autophagy to
227 remodel the proteome upon perception of wide range of treatments, among them auxin and
228 cytokinin (Rodriguez *et al*, 2020). We started by imaging the maturation zone, as ARF7 cytoplasmic
229 condensates are mostly observed in this region. We noticed that the co-localization of ARF7-Venus
230 with mCherry-ATG8a varied during the time of the day, *i.e.,* there is a significant increase (45% to
231 85%, $P<0.05$) in ARF7 and ATG8a co-localization when comparing seedlings imaged during Zeitgeber
232 time (ZT, time after the lights are switched on) ZT0 vs ZT6, respectively. This is consistent with
233 previous reports (Perianez-Rodriguez *et al*, 2021) showing that ARF7 expression follows a periodic
234 fluctuation of 4-6h in the oscillation zone. Given this, we decided to use ZT0 as the timepoint for
235 subsequent treatments. Next, we incubated seedlings with vacuolar protease inhibitors (Pepstatin A
236 and E-64d) which led to a dramatic increase in ARF7-Venus co-localization with mCherry-ATG8a (Fig
237 3C & D). This both supports our findings with *ARF7-Venus* x *atg2-1* (Figure 1) and also the
238 proposition that ARF7 condensate formation can be linked to autophagic degradation. Similarly, NAA
239 treatment promoted a significant increase of ARF7-Venus co-localization with mCherry-ATG8
240 positive foci in the cytoplasm (Fig 3 C &D) while Kinetin did not lead to increased ARF7-Venus co-
241 localization with mCherry-ATG8a ($P>0.05$). Altogether, our results suggest that ARF7 cytoplasmic
242 localization might be part of a proteome remodelling strategy which is mediated, at least in part, via
243 autophagy.

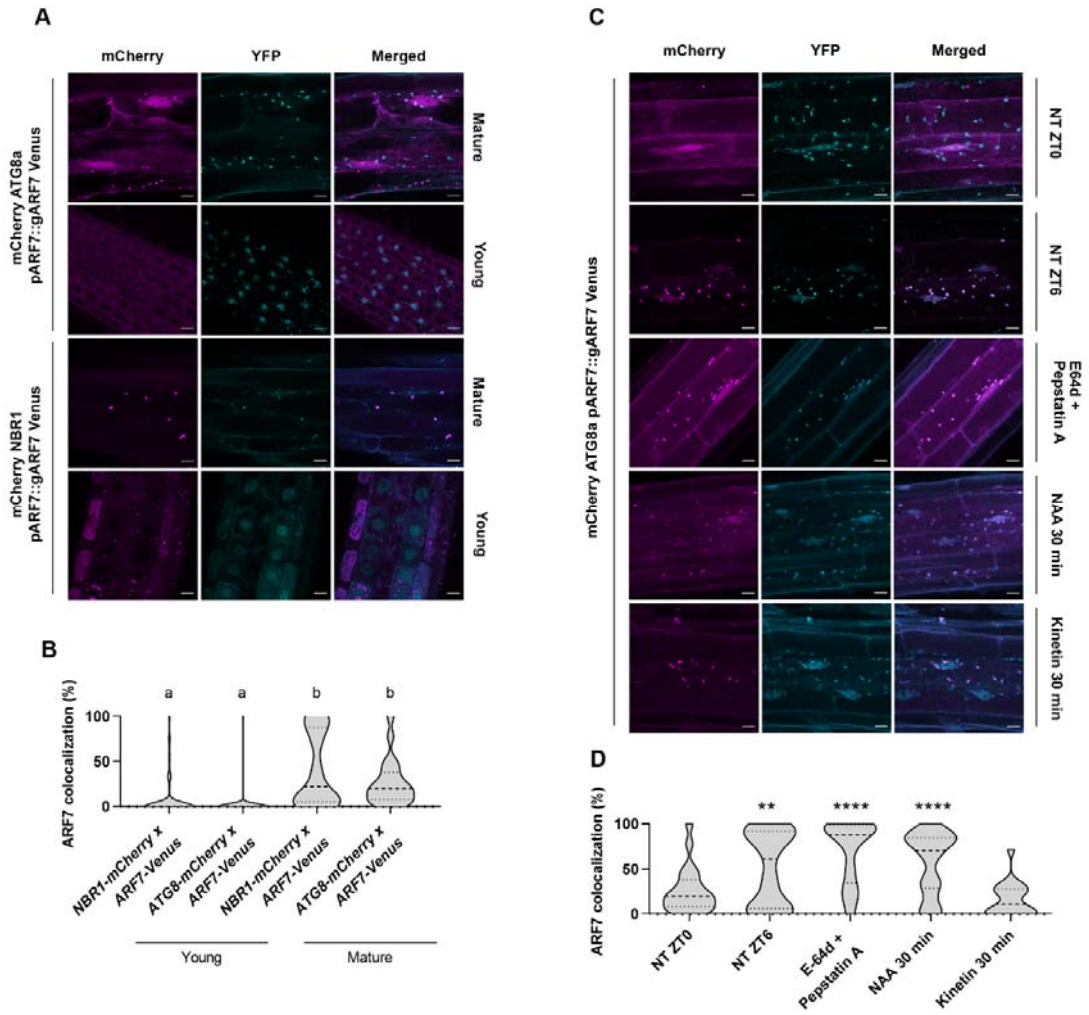

Figure 3 ARF7 co-localization with autophagosomes displays rhythmic variation and is enhanced by NAA treatment. **A**) Co-localization of ARF7-Venus with mCherry-ATG8a (nuclei and/or cytoplasmic foci) or mCherry-NBR1 (cytoplasmic foci) in young (meristem/elongation) or maturation zone. Representative pictures were taken in the differentiation zone of 10–14-day old *Arabidopsis* seedlings. Scale bar 10 µM. **B**) Quantification of the co-localization of ARF7-Venus with mCherry-ATG8a or NBR1 under conditions depicted in **A)**; samples followed by the same letters are not statistically different (Dunn's test, P≤0.0001). **C)** ARF7-Venus co-localization with autophagosomes under selected treatments: No Treatment (NT), E64d + Pepstatin A (vacuolar protease inhibitors), NAA (1µM NAA for 30 min) and Kinetin (1µM Kinetin for 30 min). Scale bar 10 µM. **D)** Quantification of the co-localization of ARF7-Venus with mCherry-ATG8a under conditions depicted in **C)**. The outline of the violin plots represents the probability of the kernel density. Dotted lines represent interquartile ranges (IQR), with the thick horizontal line representing the median; whiskers extend to the highest and lowest data point. Results were obtained from three independent experiments with at least 8 plants per condition. Asterisks mark statistical significance to NT (MS+ solvents) according to a Wilcoxon-rank test (**0.01; **** 0.0001).

Autophagy regulates rhythmic changes to ARF7 *protein abundance but is not required for PBS establishment*

260 Intrigued by our results showing that co-localization between ARF7 and ATG8a follows rhythmic
261 variation and knowing that *ARF7* expression also shows a similar pattern in the oscillation zone (OZ,
262 Perianez-Rodriguez *et al*, 2021), we decided to explore the impact of autophagy in the natural
263 variation of ARF7's abundance. Therefore, we performed western blots against ARF7 in Col-0 and
264 *atg* mutants' seedlings during a 12h period. As seen in Fig 4A, ARF7 levels increased from ZT0 to ZT9,
265 followed by progressive decline up to ZT12, which is in agreement with the abovementioned pattern
266 for *ARF7* transcript oscillation in the OZ. Moreover, these results likely explain the variation in co-
267 localization of ARF7-Venus with autophagosomes at different timepoints (Fig 3): condensation is
268 dependent on target concentration (Mcswiggen *et al*, 2019) and therefore more likely observable
269 under high ARF7 levels (ZT6). Our findings also illustrate that ARF7 abundance display rhythmic
270 changes in the whole plant, which is consistent *ARF7*'s expression profile (*e.g.,* Rosado *et al*, 2012;
271 Lee *et al*, 2019) and with ARF7's role during hypocotyl gravi- and phototropism (Wang *et al*, 2020).

272 In marked contrast, the rhythmic variation in ARF7's abundance was lost ($P \leq 0.05$) when autophagy
273 was disrupted (Fig 4B-D). Moreover, the transcript levels of *LBD16*, which is directly regulated by
274 ARF7, also lost its rhythmic fluctuation in *atg* mutants (Fig 4E). Interestingly, *LBD16* levels are
275 substantially higher in *atg2-1* than Col-0, which could be related to the overall higher levels of ARF7
276 seen in *atg* mutants. Taken together, these results demonstrate the importance of autophagy in
277 regulating ARF7-dependent rhythm.

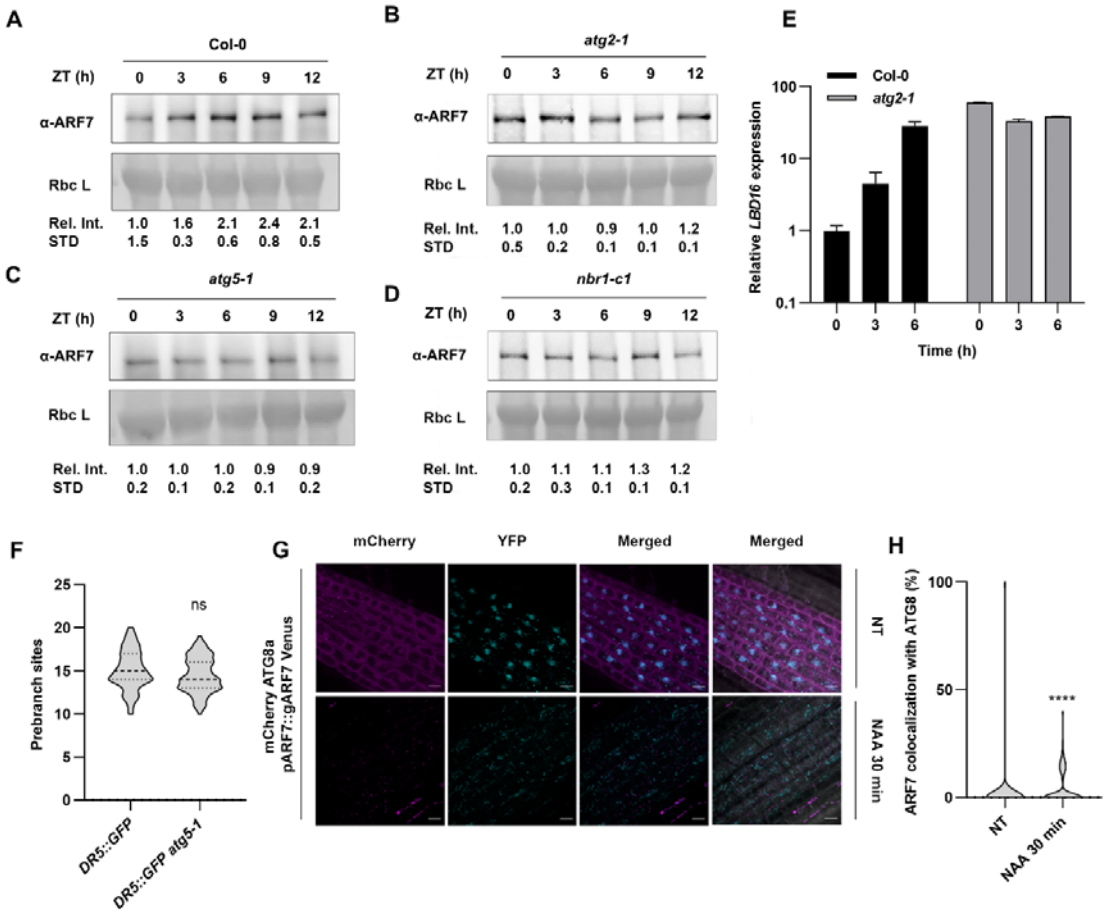

Figure 4: ARF7 abundance displays whole-plant rhythmic variation and is modulated by autophagy. **A-D)** ARF7 western blots from proteins extracted from Col-0 (**A**); *atg2-1* (**B**); *atg5-1* (**C**) or *nbr1-c1* (**D**) at given Zeitgeber time (ZT0-ZT12). Values below each band represent the relative intensity ratio between ARF7 and RuBisCO large subunit (Rbc L) as stained with Ponceau S used as loading control. Ratios were normalized to untreated Col-0 (NT) which was arbitrarily set to 1. Values given are the mean ± SD of 3 independent experiments, Col-0 was statistically significant ($P \leq 0.05$) from all autophagy mutant, according to a Paired-T-test. **E)** Relative gene expression oscillation of *LBD16* in Col-0 and *atg2-1* at given timepoints. *LBD16* expression was normalized to *ACTIN2* and set to 1 for each genotype at timepoint 0h. **F)** Prebranch site (PBS) in *DR5::GFP* and *DR5::GFP x atg5-1*. PBS of 5-day post germination, vertically grown seedlings were scored with a stereo microscope. The outline of the violin plots represents the probability of the kernel density. Dotted lines represent interquartile ranges (IQR), with the thick horizontal line representing the median; whiskers extend to the highest and lowest data point. Results were obtained from 4 independent experiments with a total of at least 80 plants per genotype. Mann-Whitney was used for the statistical test. **G)** ARF7-Venus and mCherry-ATG8a co-localization in root young tissue treated with MS + solvent (top panel) or MS+NAA (bottom panel) for 30 min. **H)** Quantification of the co-localization of ARF7-Venus with mCherry-ATG8a under conditions depicted in **G)**. The outline of the violin plots represents the probability of the kernel density. Dotted lines represent interquartile ranges (IQR), with the thick horizontal line representing the median; whiskers extend to the highest and lowest data point. Results were obtained from three independent experiments with at least 8 plants per condition. Asterisks mark statistical significance to NT according to a Mann-Whitney test (**** 0.001).

297 *ARF7* oscillation has been established as an essential step during PBS determination as *arf7-1*
298 mutants display abnormal PBS patterning (Perianez-Rodriguez *et al*, 2021). Because ARF7 abundance
299 does not seem to change when autophagy is impaired, we questioned whether PBS establishment
300 could be affected in *atg* mutants. To track this, we compared PBS numbers in Col-0 and *atg5-1* lines
301 expressing *DR5::GFP* with a stereo microscope. As seen in Fig 4F, there was no major differences in
302 PBS count (P>0.05) between both genotypes, being that the total number of PBS we report are
303 comparable to those available in the literature for Col-0 (Moreno-Risueño *et al*, 2010). Taken
304 together, our results suggest that while autophagy is necessary for ARF7´s rhythmic fluctuation,
305 deficiencies in the degradation process do not produce major interference with PBS establishment.

306

307 *Autophagy deficiency negatively impacts auxin mediated proteome remodelling*

308 Intriguingly, our results could suggest that ARF7 oscillation might not be necessary for PBS
309 establishment, which disagrees with previous reports (Perianez-Rodriguez *et al*, 2021). Several
310 explanations could justify these seemingly contradictory differences. Firstly, *ARF7*'s oscillation
311 relevance during PBS establishment was inferred from analysing *arf7-1*(Perianez-Rodriguez *et al*,
312 2021) in which there is no ARF7 expression. On the other hand, in *atg* mutants, ARF7 is expressed
313 but does not oscillate due to defective proteostasis (Fig 1-4). It could thus be possible that while
314 ARF7 is undoubtedly important for correct PBS establishment, the oscillation of this protein might
315 not be essential for the process. Alternatively, *ARF7´s* levels in the OZ zone could be regulated by
316 different mechanisms than in the rest of the plant; this would be consistent with the
317 aforementioned nucleo-cytopartitioning of ARF7 (Fig 3, Powers *et al*, 2019). To analyse this, we
318 decided to investigate auxin's effect on ARF7 and ATG8a co-localization but now focusing on
319 younger tissue. Like seen for the maturation zone (Fig 3C-D), NAA caused ARF7-Venus to massively
320 localize in cytoplasmic foci (Fig 4G); indicating that auxin promotes ARF7 condensations. Likewise,
321 we also observed a massive increase in mCherry-ATG8 foci (Fig 4G), which is consistent with our
322 previous reports showing that quick bursts of auxin lead to rapid increase in autophagic activity
323 (Rodriguez *et al*, 2020). Surprisingly, these dramatic increases of ARF7 and ATG8a cytoplasmic foci
324 only produced a modest, albeit significant, increase in co-localization (Fig 4G & H), which contrasts
325 with our maturation zone data (Fig 3). Given that a) autophagy has a well characterized role in
326 aggregate degradation (*e.g.*, Lim *et al*, 2015); b) the root meristem has been shown to display zone
327 specific chaperonin expression to prevent protein aggregation (Llamas *et al*, 2021); c) ARF7
328 condensates have liquid and solid properties (Fig EV2, Powers et al 2019); d) ARF7 condensates are
329 more prominent in older tissue (Fig3, Powers *et al*, 2019); our results here likely reveal a mechanism

330 by which auxin treatment leads to a rapid activation of autophagy to modulate ARF7 levels though
331 this mainly occurs in older tissue, where aggregation is more prone to occur.

332 In sum, these experiments reveal that while the oscillation of ARF7 abundance seems to be a whole
333 plant phenomenon, the means by which this regulation occurs might be zone specific. Likewise, this
334 apparent zone-specific regulation of ARF7 turnover also reconciles our findings with those of
335 Perianez-Rodriguez et al, 2021, namely the relevance of *ARF7* oscillation to PBS establishment and
336 the normal PBS establishment in *atg* mutants.

337 Given that NAA induced rapid ARF7 localization to cytoplasmic foci, we wondered if this would have
338 any effect in ARF7 abundance. Hence, we checked ARF7 levels by western blot with protein extracts
339 from Col-0 and *atg2-1* seedlings treated with NAA for 1h at ZT0 (Fig EV3). Our data revealed that
340 NAA produced a mild but significant decrease ($P \leq 0.01$) in ARF7 levels in Col-0, which is consistent
341 with the NAA-induced increase co-localization between ARF7 and autophagic components (Fig 3 &
342 4). In combination, our results (Fig 3-4, EV3) support a mechanism by which auxin promotes ARF7's
343 condensation to modulate ARF7 levels, preventing excessive nuclear ARF7 and consequent
344 exaggerated responses. In contrast to previous reports (e.g., Wang *et al*, 2005; Perianez-Rodriguez *et*
345 *al*, 2021), our data suggests that auxin treatment induces changes to ARF7 abundance; which has
346 also been reported at the transcript level after 2h of IAA treatment (Biswas *et al*, 2019). These
347 differences might be easily conciliated due to different experimental set ups among reports: longer
348 auxin treatments (3h-16h) and different tissues (*i.e.,* root's OZ or protoplast) were used in those
349 reports (Perianez-Rodriguez *et al*, 2021; Wang *et al*, 2005) as opposed to the experimental setup
350 used here. This is supported by our data, which indicates that tissue specific mechanisms and time of
351 the day appear to be important factors during ARF7 turnover and by predicted buffering
352 mechanisms of ARF7 signalling (Perianez-Rodriguez *et al*, 2021). Concerning *atg2-1* seedlings, NAA
353 treatment did not lead to significant changes in ARF7 levels (Fig EV3) which might not be surprising
354 given that ARF7 levels are already elevated when autophagy is impaired and that other
355 compensatory mechanisms (*e.g.*, proteasome) could be upregulated to compensate for defective
356 autophagy.

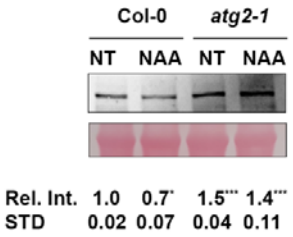

357

358 **Figure EV3** NAA-induced changes to ARF7s abundance is lost in *atg* mutant. ARF7 western blot from proteins extracted
359 from Col-0 or *atg2-1* treated with MS + solvent or MS supplemented with NAA (1µM, 60 min), at Zeitgeber time 0 (ZT0).
360 Values below each band represent the relative intensity ratio between ARF7 (**A**) and RuBisCO large subunit (Rbc L) as
361 stained with Ponceau S used as loading control. Ratios were normalized to each genotype's NT sample (MS+ solvent),
362 which was set to 1. Values are mean ± SD of 5 biological replicates. Statistical analysis was done using a Holm-Sidak test (*
363 0.05; *** 0.001).

364

365 Accumulation of ARF7 in the cytoplasm, which we have shown is impacted by autophagy (Fig 1 D-I;
366 Fig3), has been linked to decreased auxin-dependent responses (Powers *et al*, 2019). Moreover,
367 *atg2-1* is unable to execute ARF7 turnover upon rapid auxin treatment (Fig EV3) and we wondered if
368 this could be indicative of more broad implications, namely altered proteome remodelling during
369 rapid auxin enacted responses. To evaluate this, we gave a short auxin treatment (30 min) to Col-0
370 and *atg2-1* seedlings and performed Mass Spectometry (MS). Despite the rapid nature of the
371 treatment with NAA, proteome remodelling was engaged in both genotypes (Fig 5A), and as
372 expected, more proteins were downregulated in Col-0 than *atg2-1* (167 vs 94, Fig 5B). This
373 difference in auxin-induced downregulated proteins between the genotypes is consistent with the
374 loss of a major proteostasis pathway in the *atg2-1* background. There were also differences, albeit
375 smaller, in what concerns auxin-induced protein accumulation, 146 for Col-0 vs 114 for *atg2-1*.
376 Surprisingly, only around 5% of the proteins with differential regulation upon NAA treatment were
377 similarly down (or up) regulated in both genotypes. These results indicate that while *atg2-1*
378 responds to NAA, the nature of this response is substantially different to that of Col-0, both
379 supporting and expanding our previous findings (Rodriguez et al 2020) showing defective NAA-
380 induced reprogramming in *atg* mutants.

381

382 *Autophagy facilitates LR formation*

383 As our results suggest that autophagy's contribution to ARF7 turnover might be more prominent in
384 mature tissue, we wondered if accumulation of ARF7 in *atg* mutants could have an impact in other
385 ARF7-dependent phenotypes. Besides PBS, ARF7 regulatory role during LR initiation is also well
386 established (*e.g.,* Okushima *et al*, 2007; Goh *et al*, 2019); consequently, we examined *atg* mutants'
387 ability to produce LRs by transplanting 5-day old seedlings to vertical plates and scored LRs after 9
388 days (Fig 5 C-D). As shown in Fig 5, *atg* mutants have a significantly lower LR density when compared
389 to Col-0. Because we have seen that lack of autophagy leads to condensation of ARF7 (Fig 3) which
390 has been linked with decreased auxin responses (Powers *et al*, 2019) and because NAA treatment
391 did not produce major changes to ARF7 abundance in *atg2-1* seedlings (Fig EV3), we questioned if

392 *atg* mutants might have dampened auxin responses. To ascertain this, we germinated Col-0 and *atg*
393 mutants and after 5 days, transferred them to vertical MS plates with or without NAA (0.1 µM) and
394 counted LRs 9 days after germination. As seen in Fig 5 C-D, NAA treatment caused an increase in LR
395 density for all genotypes, but it did not rescue the differences observed between Col-0 and *atg*
396 mutants. These results are in agreement with our previous findings (Rodriguez *et al*, 2020) regarding
397 *atg* mutants' reduced ability to respond effectively to callus inducing media (rich in auxin) to form
398 callus, a process resembling LR initiation.

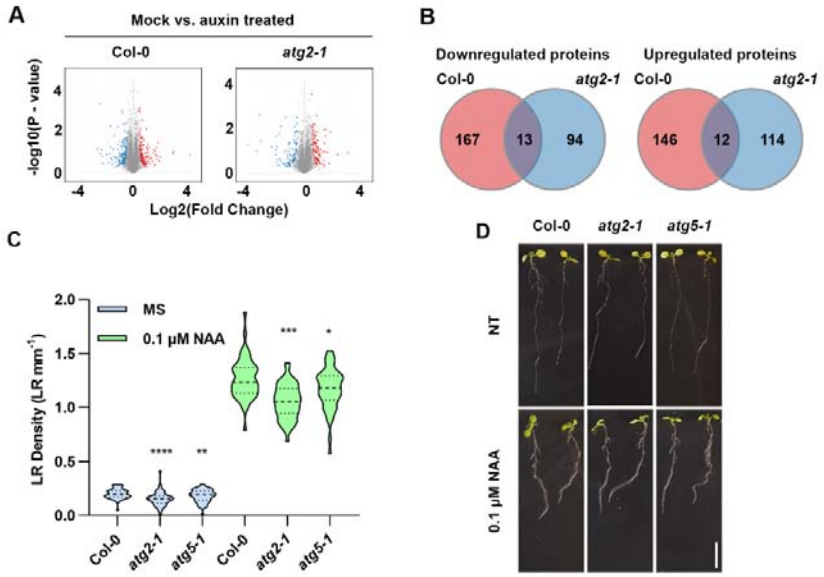

399

400 **Figure 5** Autophagy deficient mutants display impaired proteome remodelling upon auxin treatment and show decreased
401 LR formation capacity. **A)** Volcano plot displaying pairwise protein content changes in Col-0 or *atg2-1*, 30 min after Mock
402 (MS+ EtOH) or NAA treatment (MS+ NAA) with a F.D.R. <0.05 using an unpaired t-test. **B**) Venn diagrams showing the
403 number of differentially expressed proteins overlapping between the datasets (F.D.R. < 0.05). **C-D**) LR density
404 quantification in Col-0, *atg2-1* and *atg5-1* grown in MS plates supplemented with Solvent (MS) or 0.1 µM NAA. The outline
405 of the violin plots represents the probability of the kernel density. Dotted lines represent interquartile ranges (IQR), with
406 the thick horizontal line representing the median; whiskers extend to the highest and lowest data point but no more than
407 ±1.5 times the IQR from the box. Results were obtained from three independent experiments with at least 40 plants per
408 condition, asterisks mark statistical significance to Col-0 according to the t-test (*0.05; **** 0.0001). Scale bar: 1 cm

409

410

411 Discussion

412 Here, we show that autophagy modulates ARF7 and ARF19 turnover and how through the selective
413 cargo adaptor NBR1 (Fig 1 & 2). We and others (Jing *et al*, 2022) have shown that MG132 treatment

414 also causes ARF7 to accumulate, which suggests proteasomal activity also regulates this TF turnover.
415 However, care should be taken when inferring proteasomal contribution based solely on MG132-
416 derived data as this inhibitor produces several off-target effects like transcriptional upregulation
417 (Wang *et al*, 2008; Cho *et al*, 2013), interference with lysosomal proteases (Garrison & Bangs, 2020)
418 and autophagosome assembly (Ji *et al*, 2016). Nonetheless, as we see a synergistic effect of MG132
419 and autophagy inhibition in ARF7 accumulation (Fig 1), it is likely that both degradation pathways are
420 involved in regulating ARFs turnover. The recruitment of both degradation pathways to promote
421 ARF7 turnover is in line with the necessity to keep *ARF7* output under tight control (Moreno-Risueño
422 *et al*, 2010; Perianez-Rodriguez *et al*, 2021) and with the fact that excessive activating ARFs lead to
423 dramatic developmental retardation due to exaggerated auxin program execution (Powers *et al*,
424 2019). Interestingly, we find that while *atg* mutants over accumulate ARF7, autophagy blockage
425 leads to increased ARF7 cytoplasmic condensates, which have been linked to low responsiveness to
426 auxin. Consequently, despite having higher ARF7 levels than Col-0, *atg* mutants show diminished
427 auxin response (Fig EV3, Fig5), LR formation (Fig 5) and callus formation (Rodriguez *et al*, 2020), a
428 process reminiscent of LR initiation. How does accumulation of ARFs equate to diminished auxin
429 responses? It is possible that autophagy inhibition leads to ARF7 accumulation which may induce
430 supersaturation (Mcswiggen *et al*, 2019) and cause ARF7 condensation in the cytoplasm (Fig 1 & 3).
431 Recent reports (Powers *et al*, 2019; Jing *et al*, 2022) have linked ARFs condensation with decreased
432 auxin responsiveness, therefore, the disruption of protein degradation pathways we report here
433 causes ARF7 levels to increase, promoting cytoplasmic aggregation and consequent reduced auxin
434 responsiveness. While our data provides an indication that the mobilization of ARF7 to cytoplasmic
435 foci might be part of a mechanisms aimed at adjusting ARF7 abundance and auxin responsiveness,
436 more experiments are needed to fully understand this process. For instance, (Jing *et al*, 2022)
437 recently showed that the loss of function of AFF1 (F-box protein) displays reduced auxin
438 responsiveness due to cytoplasmic hyper condensation and consequent nuclear depletion of ARFs.
439 Despite these dramatic effects, the *aff1* mutants only display mild developmental phenotypes and
440 surprisingly seems able to produce LRs when supplemented with 2-4D; this contrasts with *arf7 x*
441 *arf19* mutant's severe LR formation defects, even when cultured with auxin (Okushima *et al*, 2007).
442 Moreover, we report that ARF7 cytoplasmic foci do not co-localize with autophagosomes at the
443 same extent in young vs mature tissues, even after inducing ARF7 cytoplasmic condensation with a
444 short NAA treatment (Fig 3). A caveat to this interpretation is that in young tissue, NAA-induced
445 condensates might have greater liquid-like properties, hence the lower co-location with autophagic
446 components. Given that condensate solidification is a progressive process, it is possible with time,

447 ARF7 condensates in young tissue would increase solidity and increase their co-localization with
448 ATG8a/NBR1

449 In sum, while we provide robust evidence indicating that ARF7 cytoplasmic condensation is part of a
450 triage mechanism for its autophagic degradation, further clarification is needed to completely
451 uncover how this process is regulated in different root zones.

452 In contrast to PBS establishment, which is not grossly affected in *atg5-1* (Fig 4), LR formation seems
453 to be impaired in *atg* mutants (Fig 5). In the context of LR formation, there is evidence of autophagic
454 participation in a wide range of processes like cell death regulation of endodermal cells above LRPs
455 (Escamez *et al*, 2020) and potentially also during PIN's degradation (Kleine-Vehn *et al*, 2008).
456 Moreover, autophagy modulates proteome turnover induced by different hormones like auxin (Fig
457 5; Rodriguez et al 2020), cytokinin (Acheampong *et al*, 2020; Rodriguez *et al*, 2020) and ABA
458 (Rodriguez *et al*, 2020); all of which are known to influence LR formation. For these reasons,
459 deficiencies in such a transversal process like autophagy complicate result interpretation and
460 ascribing phenotypes to a specific function of autophagy. For instance, ABA is known to interfere
461 with LRs formation (de Smet *et al*, 2003) and consequently, misregulation of ABA signalling in *atg*
462 mutants (Rodriguez *et al*, 2020) could be a source of defective LR formation. However, we have
463 previously seen that *atg* mutants have difficulties forming callus (Rodriguez *et al*, 2020) a process
464 resembling LR initiation and because ABA does not affect callogenesis (Sugimoto *et al*, 2010), it is
465 plausible that LR deficiencies in *atg* mutants occur at an earlier stage than ABA-induced effects (LR
466 emergence). Nonetheless, because our results unequivocally show that autophagy specifically
467 impacts the turnover of the important LR regulators ARF7 and ARF19, it is undeniable that at the
468 very least, defective ARFs turnover in *atg* mutants must contribute to the decreased auxin responses
469 and LR formation we report here.

470 In conclusion, we have uncovered a novel role for selective autophagy during post embryonic organ
471 development through the turnover of the key developmental regulators ARF7 and ARF19 and
472 provided further insight into the intricate mechanisms behind ARFs fine-tuning and how this affects
473 root architecture.

474

Acknowledgements

This work was funded by a Danish Research Agency grant to E.R. (DFF1- 1032-00249B). We would like to thank Tom Guilfoyle (anti-ARF7 antibody), Koki Yoshimoto (anti-ATG8a antibody), Malcolm Bennett (*pARF7::gARF7-Venus*), Yasin Dagdas (*DR5::GFP* and *atg5-1 DR5::GFP*), Liwen Jiang (*NBR1-C1*) and Hidehiro Fukaki (*pARF19::ARF19-GFP nph4-1 arf19-1*) for sharing material/reagents. Thanks are due to Miguel Moreno-Risueño and Nuria Coll for insightful discussion. We would also like to thank Suksawad Vongvisuttikun for technical assistance, the 2022 classes from the courses "Plant Molecular Biology" & "Experimental Higher Model Organisms" (University of Copenhagen, Denmark) for performing the ARF19-GFP & ARF7-Venus western blots, respectively. Confocal microscopy imaging was performed using equipment from the Center for Advanced Bioimaging (CAB) Denmark, University of Copenhagen. Mass spectrometry analyses were performed by the Proteomics Research Infrastructure (PRI) at the University of Copenhagen (UCPH), supported by the Novo Nordisk Foundation (NNF) (grant agreement number NNF19SA0059305).

Author contributions

Conceptualization: ER; Investigation: ER, EE, JA, JC, PC. Formal analyses: ER, EE, JA. Writing: ER, EE, JA Visualization: ER, JA; Supervision: ER; Funding acquisition ER. All authors read the manuscript and agreed with the findings reported.

494 **Methods and Materials**

495 *Plant material and phenotypic characterization*

496 *Arabidopsis* seedlings were grown on solid, half-strength MS media (0.8% agar, 1% sucrose at 5.7 pH)
497 and kept at 21 C° with a photoperiod of 16 h (120 µE/m^2/s). Seeds were sterilized with 1.3% bleach
498 followed by 70% alcohol and then rinsed three times with sterilized water. The following lines were
499 used throughout this study; Col-0, *atg2-1* (SALK_076727), *atg5-1* (SAIL_129_B07), *nbr1-c1* (Ji *et al*,
500 2020), mCherry ATG8a & mCherry NBR1 (Svenning *et al*, 2011), pARF7::gARF7 Venus (Orosa-Puente
501 *et al*, 2018), pARF19::ARF19-GFP/*nph4-1 arf19-1* (Okushima *et al*, 2007), DR5::GFP and DR5::GFP
502 *atg5-1* (Gift from Yasin Dagdas, GMI Vienna, Austria).

503 For the time course experiments, seedlings were acclimated in liquid half-strength MS media for at
504 least 2 days before sampling. Sampling was done just before the chamber light was turned on ZT0,
505 and then at indicated times. For LR and PBS scoring, seedlings were germinated on half-strength MS
506 media and set to grow vertically for the indicated time, using a Leica M165 FC stereomicroscope.
507 PBSs were counted after 7 days using GFP filter to visualize DR5 driven, GFP signal. Per genotype, at
508 least 70 plants were analyzed derived from 6 independent experiments. LR's were counted at day 9
509 as described by (Dubrovsky & Forde, 2012), and only LR's that had at least reached stage IV were
510 included. Per genotype/condition at least 40 plants were counted derived 6 independent
511 experiment. All genotypes were blinded during counting in both assays to prevent potential bias.

512 *Chemical treatments*

513 For confocal microscopy and western blot assays, seedlings were acclimated in liquid half-strength
514 MS media for 2 days acclimation before imaging. For hormone treatment effect on the co-
515 localization of ARF7 with ATG8 & NBR1, samples were either treated with NAA (1 µM), Kinetin (1
516 µM), or MS for the given time. Chemical inhibition of autophagy was done by pre-treating seedlings
517 with the vacuolar protease inhibitors E-64d (1:3000, stock 10 µM) and Pepstatin A (1 µM) 16 h prior
518 imaging or western blotting. For inhibition of condensates in the mature regions of the root, roots
519 were imaged just before and directly after treatment with condensate inhibitor 1,6-hexanediol
520 (10%) as described by(Wang *et al*, 2021). Images were taken at 5 min interval for 30 min. Confocal
521 imaging of the seedlings was taken with LSM700 Zeiss confocal microscope, at 20x or 63x water
522 objective. Images were analyzed using Zen 2012 (Zeiss).

523 For protein analysis of ARF7 in *atg* mutants upon proteasomal blockage, samples were treated with
524 or without MG132 (100 µM) for 16 h before harvest.

525

526 *Protein extraction*

527 Proteins were extracted using 3xSDS buffer (30% glycerol, 3% SDS, 94 nM Tris, pH 6.8, Bromophenol
528 blue, Complete ultra-tablets EDTA-free protease inhibitor cocktail (Roche), 50mM DTT), then
529 samples were centrifugated for 20 min at 4°C 14000 rpm and the supernatant was moved into a new
530 tube. Samples were denatured at 95°C for 5 min before loaded it for SDS-PAGE.

531 *SDS-PAGE and western blotting*

532 Protein samples were separated in a 4-20% pre-casted gel (Bio-Rad) and transferred overnight onto
533 nitrocellulose membrane (GE Healthcare). Membranes were blocked for 1 h with 5% skim milk
534 (Merck) in TBST [50 mM Tris-HCL, pH 7.5 150 nM NaCl, 0.1% Tween-20 (Sigma)] and incubated 2 h at
535 room temperature or overnight (4°C) with primary antibodies: anti-ARF7 (Wang et al, 2005), anti-
536 NBR1 (AS14 2805, Agrisera; 1:5000); anti-GFP (TP401 AMSBio, 1:1000); anti-ATG8a (Yoshimoto *et al*,
537 2004) Membranes were washed, followed by incubation in anti-rabbit HRP conjugate (Promega;
538 1:5000). Home-made chemiluminescent substrate (Mruk & Cheng, 2011) was applied before
539 detection. Bands were quantified using ImageJ and normalized to loading controls.

540 *Sample preparation for proteomic analysis*

541 Tissue extracts (100 µg) were diluted in digestion buffer (0.5% SDC in 50 mM TEAB), heat-treated for
542 5 min at 95 °C, and prepared by a modified filter-aided sample preparation (FASP) protocol (65). In
543 brief, tissue extracts were transferred to 0.5 ml (tilted) spin filters (Amicon), centrifuged at 14,000g
544 for 15 min, and reduced and alkylated by addition of digestion buffer containing 1:50 (v:v) tris(2-
545 carboxyethyl)phosphine (0.5 M, Sigma) and 1:10 (v:v) 2-chloroacetamide (Sigma) for 30 min at 37 °C.
546 Samples were digested in fresh digestion buffer containing 1 µg Typsin/LysC mix (Promega) and
547 0.01% ProteaseMAX (Promega) O/N at 37 °C. Digested samples were desalted using stage-tips
548 containing styrene divinylbenzene reversed-phase sulfonate material (SDB-RPS; 3 M).

549 The mesenteric artery-based library was generated using a pooled digested and stage-tipped sample
550 from the 12-week-old SHRs and WKYs that was fractionated. A high-pH reverse-phase peptide (HpH)
551 fractionation kit (Pierce, Thermo Scientific) was used to create the 15 fractionations.

552 *Data acquisition by liquid chromatography–mass spectrometry (LC-MS)*

553 Peptides were separated on 50 cm columns packed with ReproSil-Pur C18-AQ 1.9 µm resin (Dr
554 Maisch GmbH). Liquid chromatography was performed on an EASY-nLC 1200 ultra-high-pressure
555 system coupled through a nanoelectrospray source to an Exploris 480 mass spectrometer (Thermo
556 Fisher Scientific). Peptides were loaded in buffer A (0.1% formic acid) and separated applying a

557 nonlinear gradient of 5 to 65% buffer B (0.1% formic acid, 80% acetonitrile) at a flow rate of 300
558 nl/min over 100 min. Spray voltage was set to 2400 V. Data acquisition switched between a full scan
559 (120,000 resolution, 45 ms max. injection time, AGC target 300%) and 49 DIA scans with isolation
560 width of 13.7 m/z and windows overlap of 1 m/z spanning a precursor mass range of 361 to 1033
561 m/z (15,000 resolution, 22 ms max. injection time, AGC target 1000%). Normalized collision energy
562 was set to 27. All statistical analysis of LFQ derived protein expression data was performed using the
563 automated analysis pipeline of the Clinical Knowledge Graph (Santos *et al*, 2022).

564 *Data availability*

565 The mass spectrometry data from this publication has been deposited to the PRIDE archive (Perez-
566 Riverol et al 2022; https://www.ebi.ac.uk/pride/archive/) and given the identifier [PXD042834]

567 *Vector construction and Plant Transformation for BiFC*

568 To create pDEST-ATG8a-SCYNE, pDEST-NBR1-SCYCE, pDEST-ARF7-VYNE and pDEST-TSPO-SCYCE, we
569 PCR amplified (CloneAMP HIFI PCR premix, TAKARA) the coding sequences of *ATG8a*, *NBR1*, *ARF7*
570 *and TSPO* flanked recognition sequence for Gateway (Thermofischer) or In-Fusion (Clontech) cloning.
571 *ATG8a, NBR1 and ARF7's* PCR products were cloned into pENTR (Life Technologies) and
572 subsequentially transferred (LR clonase, Invitrogen) into the Gateway-compatible BiFC vectors (Gehl
573 C *et al*, 2009) pDEST-^{GW} SCYNE, pDEST-^{GW}SCYCE, pDEST-^{GW}VYNE. *TSPO* PCR amplicon was directly
574 cloned into pDEST-^{GW}SCYCE using In-Fusion cloning. *Agrobacterium* strain GV3101 containing
575 constructs were grown in Yeast-extract peptone media supplied with the respective antibiotics
576 overnight. Cultures were spun and resuspended in 10mM $MgCl_2$, 10 mM MES-K and 100 µM
577 acetosyringone to the density of 600nm = 0.15-0.2 per construct and mixed 1:1 and left at room
578 temperature for 2 h, followed by infiltration in 3 weeks old *N. Benthamiana*. Pictures were taken 48
579 hpi using a Zeiss LSM 700 confocal microscope.

580 *Immunoprecipitation*

581 Immunoprecipitation assay was described previously (Zuo *et al*, 2022). In brief, 1 g of 14-day old
582 seedlings were grinded with mortar and pestle and 2 ml of IP extraction buffer (50mM Tris-HCl pH
583 7.5, 150mM NaCl, 5% glycerol 1mM EDTA, 0.1% NP40, 10mM DTT, protease inhibitor (mini complete
584 ultra, EDTA-free) was added, followed by centrifugation at 4°C 13000 rpm, 20 min. The supernatant
585 was incubated with 20 µl GFP trap beads (Chromotek) rotating for 2-4-hours at 4°C. The beads were
586 washed 3-4 times with washing buffer (20 mM Tris-HCl pH 7.5, 0.15 M NaCl, 0.1% NP40). 30 µL of
587 3xSDS was added to the beads and heat up 5 min at 95 °C before proceeding for SDS-PAGE.

588 *RNA extraction*

589 RNA was extracted as described previously (Zuo *et al*, 2022) using TRIzol reagent (Thermo Scientific),
590 treated with DNase (Thermo Scientific) and was reverse transcribed into cDNA using Reverse Aid kit
591 (Thermo Scientific) as described by the manufacturer. qPCR assays were executed on the
592 Quantstudio 1 (Applied Biosystems) system using SYBR Green master mix (ThermoFisher), *ACT2* was
593 used as internal control. All primers used for qPCR analysis are listed in Supplementary table 1. The
594 experiment was repeated three times.

595 **Supplementary table 1**

Cloning primers	
ARF7 Forward primer	5'-CACCATGAAAGCTCCTTCATCAA-3'
ARF7 Reverse primer	5'-TCACCGGTTAAACGAAGTGGC-3'
NBR1 Forward primer	5'-CACCATGGAGTCTACTGCTA-3'
NBR1 Reverse primer	5'-TCAAGCCTCCTTCTCCCCT-3'
TSPO Forward primer	5'-GCAGGCTCCGCGGCCATGGATTCTCAGGACATCAGA-3'
TSPO Reverse primer	5'-AGCTGGGTCGGCGCGTCACGCGACTGCAAGCTTTAC-3'
ATG8a Forward	5'-CACCATGATCTTTGCTTGCTTGA-3'
ATG8a Reverse	5'-TCATCAAGCAACGGTAAGAGAT-3'
qPCR primers	
ACT2 Forward primer	5'-CTTGTTCCAGCCCTCGTTTGTG-3'
ACT2 Reverse primer	5'-CCTTGGAGATCCACATCTGCTG-3'
ARF7 Forward primer	5'-CAAGGTCACAGTGAGCAAGTCG -3'
ARF7 Reverse primer	5'-TGTGGAGCATGCATATGAGCTTGG -3'
LBD16 Forward primer	5'-TCCATGATCGATGTGAAGCTGTCG-3'
LBD16 Reverse primer	5'-TGTGATTGCAAGAAAGCCACCTG-3'

596

597

598

599

600 **References**

601 Bassham DC, Laporte M, Marty F, Moriyasu Y, Ohsumi Y, Olsen LJ & Yoshimoto K (2006)
602 Autophagy in development and stress responses of plants. *Autophagy* 2: 2–11

603 Biswas MS, Fukaki H, Mori IC, Nakahara K & Ichi Mano J' (2019) Reactive oxygen species and
604 reactive carbonyl species constitute a feed-forward loop in auxin signaling for lateral root
605 formation. *The Plant Journal* 100: 536–548

606 Chen L, Liao B, Qi H, Xie LJ, Huang L, Tan WJ, Zhai N, Yuan LB, Zhou Y, Yu LJ, *et al* (2015)
607 Autophagy contributes to regulation of the hypoxia response during submergence in
608 Arabidopsis thaliana. *Autophagy* 11: 2233–2246

609 Cho KS, Kwon KJ, Jeon SJ, Joo SH, Kim KC, Cheong JH, Bahn GH, Kim HY, Han SH, Shin CY, *et al*
610 (2013) Transcriptional Upregulation of Plasminogen Activator Inhibitor-1 in Rat Primary
611 Astrocytes by a Proteasomal Inhibitor MG132. *Biomol Ther (Seoul)* 21: 107

612 Deb S, Sankaranarayanan S, Wewala G, Widdup E & Samuel MA (2014) The S-Domain Receptor
613 Kinase Arabidopsis Receptor Kinase2 and the U Box/Armadillo Repeat-Containing E3
614 Ubiquitin Ligase9 Module Mediates Lateral Root Development under Phosphate
615 Starvation in Arabidopsis. *Plant Physiol* 165: 1647–1656

616 Desideri E, Filomeni G & Ciriolo MR (2012) Glutathione participates in the modulation of
617 starvation-induced autophagy in carcinoma cells. *Autophagy* 8: 1769–1781

618 Du Y & Scheres B (2018) Lateral root formation and the multiple roles of auxin. *J Exp Bot* 69:
619 155–167

620 Dubrovsky JG & Forde BG (2012) Quantitative analysis of lateral root development: Pitfalls and
621 how to avoid them. *Plant Cell* 24: 4–14

622 Escamez S, André D, Sztojka B, Bollhöner B, Hall H, Berthet B, Voß U, Lers A, Maizel A,
623 Andersson M, *et al* (2020) Cell Death in Cells Overlying Lateral Root Primordia Facilitates
624 Organ Growth in Arabidopsis. *Current Biology* 30: 455-464.e7

625 Fujioka Y, Alam JM, Noshiro D, Mouri K, Ando T, Okada Y, May AI, Knorr RL, Suzuki K, Ohsumi Y,
626 *et al* (2020) Phase separation organizes the site of autophagosome formation. *Nature*
627 578: 301–305

628 Garrison P & Bangs JD (2020) p97 Inhibitor CB-5083 Blocks ERAD in Trypanosoma brucei. *Mol*
629 *Biochem Parasitol* 239

630 Gehl C, Waadt R, Kudla J, Mendel R & Hansch R (2009) New GATEWAY vectors for high
631 throughput analyses of protein-protein interactions by bimolecular fluorescence
632 complementation. *Mol Plant*: 1051–1058

633 Goh T, Toyokura K, Yamaguchi N, Okamoto Y, Uehara T, Kaneko S, Takebayashi Y, Kasahara H,
634 Ikeyama Y, Okushima Y, *et al* (2019) Lateral root initiation requires the sequential
635 induction of transcription factors LBD16 and PUCHI in Arabidopsis thaliana. *New*
636 *Phytologist* 224: 749–760

637 Hachez C, Veljanovski V, Reinhardt H, Guillaumot D, Vanhee C, Chaumont F & Batoko H (2014)
638 The Arabidopsis abiotic stress-induced TSPO-Related protein reduces cell-surface

639 expression of the aquaporin PIP2;7 through protein-protein interactions and autophagic
640 degradation. *Plant Cell* 26: 4974–4990

641 Hafrén A, Macia J-L, Love AJ, Milner JJ, Drucker M & Hofius D (2017) Selective autophagy limits
642 cauliflower mosaic virus infection by NBR1-mediated targeting of viral capsid protein and
643 particles. *Proceedings of the National Academy of Sciences* 114: E2026–E2035

644 Hofius D, Schultz-Larsen T, Joensen J, Tsitsigiannis DI, Petersen NHTT, Mattsson O, Jørgensen
645 LB, Jones JDGG, Mundy J & Petersen M (2009) Autophagic Components Contribute to
646 Hypersensitive Cell Death in Arabidopsis. *Cell* 137: 773–783

647 Huang H, Kawamata T, Horie T, Tsugawa H, Nakayama Y, Ohsumi Y & Fukusaki E (2015) Bulk
648 RNA degradation by nitrogen starvation-induced autophagy in yeast. *EMBO J* 34: 154

649 Huang L, Yu LJ, Zhang X, Fan B, Wang FZ, Dai YS, Qi H, Zhou Y, Xie LJ & Xiao S (2019) Autophagy
650 regulates glucose-mediated root meristem activity by modulating ROS production in
651 Arabidopsis. *Autophagy* 15: 407–422

652 Jacomin AC, Samavedam S, Promponas V & Nezis IP (2016) iLIR database: A web resource for
653 LIR motif-containing proteins in eukaryotes. *Autophagy* 12: 1945–1953

654 Ji C, Zhou J, Guo R, Lin Y, Kung C-H, Hu S, Ng WY, Zhuang X & Jiang L (2020) AtNBR1 Is a
655 Selective Autophagic Receptor for AtExo70E2 in Arabidopsis. *Plant Physiol* 184: 777–791

656 Ji MM, Lee JM, Mon H, Xu J, Tatsuke T & Kusakabe T (2016) Proteasome inhibitor MG132
657 impairs autophagic flux through compromising formation of autophagosomes in Bombyx
658 cells. *Biochem Biophys Res Commun* 479: 690–696

659 Jing H, Korasick DA, Emenecker RJ, Morffy N, Wilkinson EG, Powers SK & Strader LC (2022)
660 Regulation of AUXIN RESPONSE FACTOR condensation and nucleo-cytoplasmic
661 partitioning. *Nat Commun* 13: 4015

662 Kanne J V., Ishikawa M, Bressendorff S, Ansbøl J, Hasebe M, Rodriguez E & Petersen M (2021)
663 Overexpression of ATG8/LC3 enhances wound-induced somatic reprogramming in
664 Physcomitrium patens. *Autophagy* 18: 1463–1466

665 Kirkin V, Lamark T, Sou YS, Bjørkøy G, Nunn JL, Bruun JA, Shvets E, McEwan DG, Clausen TH,
666 Wild P, *et al* (2009) A Role for NBR1 in Autophagosomal Degradation of Ubiquitinated
667 Substrates. *Mol Cell* 33: 505–516

668 Kleine-Vehn J, Leitner J, Zwiewka M, Sauer M, Abas L, Luschnig C & Friml J (2008) Differential
669 degradation of PIN2 auxin efflux carrier by retromer-dependent vacuolar targeting.
670 *Proceedings of the National Academy of Sciences of the USA* 105: 17812–17817

671 Lee HW, Cho C, Pandey SK, Park Y, Kim M-J & Kim J (2019) LBD16 and LBD18 acting
672 downstream of ARF7 and ARF19 are involved in adventitious root formation in
673 Arabidopsis. *BMC Plant Biology* 19: 1–11

674 Levine B & Klionsky DJ (2004) Development by Self-Digestion. *Dev Cell* 6: 463–477

675 Lim J, Lachenmayer ML, Wu S, Liu W & Kundu M (2015) Proteotoxic Stress Induces
676 Phosphorylation of p62 / SQSTM1 by ULK1 to Regulate Selective Autophagic Clearance of
677 Protein Aggregates. 1–28

678 Liu EY, Xu N, O'Prey J, Lao LY, Joshi S, Long JS, O'Prey M, Croft DR, Beaumatin F, Baudot AD, *et*
679 *al* (2015) Loss of autophagy causes a synthetic lethal deficiency in DNA repair.
680 *Proceedings of the National Academy of Sciences* 112: 773–778

681 Liu Y, Xiong Y & Bassham DC (2009) Autophagy is required for tolerance of drought and salt
682 stress in plants. *Autophagy* 5: 954–963

683 Llamas E, Torres-Montilla S, Lee HJ, Barja MV, Schlimgen E, Dunken N, Wagle P, Werr W,
684 Zuccaro A, Rodríguez-Concepción M, *et al* (2021) The intrinsic chaperone network of
685 Arabidopsis stem cells confers protection against proteotoxic stress. *Aging Cell* 20: 1–12

686 Lv B, Wei K, Hu K, Tian T, Zhang F, Yu Z, Zhang D, Su Y, Sang Y, Zhang X, *et al* (2021) MPK14-
687 mediated auxin signaling controls lateral root development via ERF13-regulated very-
688 long-chain fatty acid biosynthesis. *Mol Plant* 14: 285–297

689 Mcswiggen DT, Mir M, Darzacq X & Tjian R (2019) Evaluating phase separation in live cells:
690 diagnosis, caveats, and functional consequences. *Genes Dev* 33: 1619–1634

691 Moreno-Risueño MA, Van Norman JM, Moreno A, Zhang J, Ahnert SE & Benfey PN (2010)
692 Oscillating Gene Expression Determines Competence for Periodic Arabidopsis Root
693 Branching. *Science (1979)* 329: 1306–1311

694 Mruk DD & Cheng CY (2011) Enhanced chemiluminescence (ECL) for routine immunoblotting.
695 *Spermatogenesis* 1: 121–122

696 Munch D, Rodriguez E, Bressendorff S, Park OK, Hofius D & Petersen M (2014) Autophagy
697 deficiency leads to accumulation of ubiquitinated proteins, ER stress, and cell death in
698 Arabidopsis. *Autophagy* 10: 1579–1587

699 Nolan TM, Brennan B, Yang M, Chen J, Zhang M, Li Z, Wang X, Bassham DC, Walley J & Yin Y
700 (2017) Selective Autophagy of BES1 Mediated by DSK2 Balances Plant Growth and
701 Survival. *Dev Cell* 41: 33-46.e7

702 Okushima Y, Fukaki H, Onoda M, Theologis A & Tasaka M (2007) ARF7 and ARF19 regulate
703 lateral root formation via direct activation of LBD/ASL genes in Arabidopsis. *Plant Cell* 19:
704 118–130

705 Orosa-Puente B, Leftley N, von Wangenheim D, Banda J, Srivastava AK, Hill K, Truskina J,
706 Bhosale R, Morris E, Srivastava M, *et al* (2018) Root branching toward water involves
707 posttranslational modification of transcription factor ARF7. *Science* 362: 1407–1410

708 Perez-Riverol Y, Bai J, Bandla C, Hewapathirana S, García-Seisdedos D, Kamatchinathan S,
709 Kundu D, Prakash A, Frericks-Zipper A, Eisenacher M, Walzer M, Wang S, Brazma A,
710 Vizcaíno JA (2022). The PRIDE database resources in 2022: A Hub for mass spectrometry-
711 based proteomics evidences. Nucleic Acids Res 50(D1):D543-D552.

712 Perianez-Rodriguez J, Rodriguez M, Marconi M, Bustillo-Avendaño E, Wachsman G, Sanchez-
713 Corrionero A, De Gernier H, Cabrera J, Perez-Garcia P, Gude I, *et al* (2021) An auxin-
714 regulable oscillatory circuit drives the root clock in Arabidopsis. *Sci Adv* 7

715 Powers SK, Holehouse AS, Korasick DA, Schreiber KH, Clark NM, Jing H, Emenecker R, Han S,
716 Tycksen E, Hwang I, *et al* (2019) Nucleo-cytoplasmic Partitioning of ARF Proteins Controls
717 Auxin Responses in Arabidopsis thaliana. *Mol Cell* 76: 177–190

718 Rodriguez E, Chevalier J, Olsen J, Ansbøl J, Kapousidou V, Zuo Z, Svenning S, Loefke C, Koemeda
719 S, Drozdowskyj PS, *et al* (2020) Autophagy mediates temporary reprogramming and
720 dedifferentiation in plant somatic cells. *EMBO J* 39: e103315

721 Rosado A, Li R, van de Ven W, Hsu E & Raikhel N V. (2012) Arabidopsis ribosomal proteins
722 control developmental programs through translational regulation of auxin response
723 factors. *Proceedings of the National Academy of Sciences* 109: 19537–19544

724 Santos A, Colaço AR, Nielsen AB, Niu L, Strauss M, Geyer PE, Coscia F, Albrechtsen NJW, Mundt
725 F, Jensen LJ, *et al* (2022) A knowledge graph to interpret clinical proteomics data. *Nat*
726 *Biotechnol* 40: 692–702

727 Scott RC, Schuldiner O & Neufeld TP (2004) Role and Regulation of Starvation-Induced
728 Autophagy in the Drosophila Fat Body. *Dev Cell* 7: 167–178

729 Sedaghatmehr M, Thirumalaikumar VP, Kamranfar I, Marmagne A, Masclaux-Daubresse C &
730 Balazadeh S (2019) A regulatory role of autophagy for resetting the memory of heat stress
731 in plants. *Plant Cell Environ* 42: 1054–1064

732 Stephani M, Picchianti L, Gajic A, Beveridge R, Skarwan E, Hernandez VS de M, Mohseni A,
733 Clavel M, Zeng Y, Naumann C, *et al* (2020) A cross-kingdom conserved ER-phagy receptor
734 maintains endoplasmic reticulum homeostasis during stress. *Elife* 9: 1–105

735 Sugimoto K, Jiao Y & Meyerowitz EM (2010) Arabidopsis Regeneration from Multiple Tissues
736 Occurs via a Root Development Pathway. *Dev Cell* 18: 463–471

737 Svenning S, Lamark T, Krause K & Johansen T (2011) Plant NBR1 is a selective autophagy
738 substrate and a functional hybrid of the mammalian autophagic adapters NBR1 and
739 p62/SQSTM1. *Autophagy* 7: 993–1010

740 Tarnowski L, Rodriguez MC, Brzywczy J, Piecho-Kabacik M, Krčkova Z, Martinec J, Wawrzynska
741 A & Sirko A (2020) A selective autophagy cargo receptor NBR1 modulates abscisic acid
742 signalling in Arabidopsis thaliana. *Sci Rep* 10: 7778

743 Turco E, Savova A, Gere F, Ferrari L, Romanov J, Schuschnig M, Martens S & Savova A (2021)
744 Reconstitution defines the roles of p62, NBR1 and TAX1BP1 in ubiquitin condensate
745 formation and autophagy initiation. *Nat Commun* 12: 5212

746 Ulmasov T, Hagen G & Guilfoyle TJ (1997) ARF1, a transcription factor that binds to auxin
747 response elements. *Science (1979)* 276: 1865–1868

748 Vanhee C, Zapotoczny G, Masquelier D, Ghislain M & Batoko H (2011) The Arabidopsis
749 Multistress Regulator TSPO Is a Heme Binding Membrane Protein and a Potential
750 Scavenger of Porphyrins via an Autophagy-Dependent Degradation Mechanism. *Plant Cell*
751 23: 785–805

752 Wachsman G, Zhang J, Moreno-Risueño MA, Anderson CT & Benfey PN (2020) Cell wall
753 remodeling and vesicle trafficking mediate the root clock in *Arabidopsis*. *Science (1979)*
754 370: 819–823

755 Wang HQ, Liu HM, Zhang HY, Guan Y & Du ZX (2008) Transcriptional upregulation of BAG3
756 upon proteasome inhibition. *Biochem Biophys Res Commun* 365: 381–385

757 Wang S, Tiwari SB, Hagen G & Guilfoyle TJ (2005) AUXIN RESPONSE FACTOR7 Restores the
758 Expression of Auxin-Responsive Genes in Mutant Arabidopsis Leaf Mesophyll Protoplasts.
759 *Plant Cell* 17: 1979–1993

760 Wang X, Jiang B, Gu L, Gu L, Chen Y, Mora M, Zhu M, Noory E, Wang Q & Lin C (2021) A
761 photoregulatory mechanism of the circadian clock in Arabidopsis. *Nat Plants* 7: 1397–
762 1408

763 Wang X, Yu R, Wang J, Lin Z, Han X, Deng Z, Fan L, He H, Deng XW & Chen H (2020) The
764 Asymmetric Expression of SAUR Genes Mediated by ARF7/19 Promotes the Gravitropism
765 and Phototropism of Plant Hypocotyls. *Cell Rep* 31: 107529

766 Wu J, Michaeli S, Picchianti L, Dagdas Y, Galili G & Peled-Zehavi H (2021) ATI1 (ATG8-interacting
767 protein 1) and ATI2 define a plant starvation-induced reticulophagy pathway and serve as
768 MSBP1/MAPR5 cargo receptors. *Autophagy* 17: 3375–3388

769 Xie D, Chen M, Niu J, Wang L, Li Y, Fang X, Li P & Qi Y (2021) Phase separation of SERRATE
770 drives dicing body assembly and promotes miRNA processing in Arabidopsis. *Nat Cell Biol*
771 23: 32–39

772 Yoshii SR, Kuma A, Akashi T, Hara T, Yamamoto A, Kurikawa Y, Itakura E, Tsukamoto S, Shitara
773 H, Eishi Y, *et al* (2016) Systemic Analysis of Atg5-Null Mice Rescued from Neonatal
774 Lethality by Transgenic ATG5 Expression in Neurons. *Dev Cell* 39: 116–130

775 Zhang Y, Yan L, Zhou Z, Yang P, Tian E, Zhang K, Zhao Y, Li Z, Song B, Han J, *et al* (2009) SEPA-1
776 Mediates the Specific Recognition and Degradation of P Granule Components by
777 Autophagy in C. elegans. *Cell* 136: 308–321

778 Zhou J, Wang J, Cheng Y, Chi YJ, Fan B, Yu JQ & Chen Z (2013a) NBR1-Mediated Selective
779 Autophagy Targets Insoluble Ubiquitinated Protein Aggregates in Plant Stress Responses.
780 *PLoS Genet* 9: 1004477

781 Zhou J, Wang J, Cheng Y, Chi YJ, Fan B, Yu JQ & Chen Z (2013b) NBR1-Mediated Selective
782 Autophagy Targets Insoluble Ubiquitinated Protein Aggregates in Plant Stress Responses.
783 *PLoS Genet* 9: 1004477

784 Zhou J, Zhang Y, Qi J, Chi Y, Fan B, Yu JQ & Chen Z (2014) E3 Ubiquitin Ligase CHIP and NBR1-
785 Mediated Selective Autophagy Protect Additively against Proteotoxicity in Plant Stress
786 Responses. *PLoS Genet* 10: e1004116

787 Zuo Z, Roux M, Rodriguez E & Petersen M (2022) mRNA Decapping Factors LSM1 and PAT
788 Paralogs Are Involved in Turnip Mosaic Virus Viral Infection. *Molecular Plant-Microbe*
789 *Interactions* 5: 125–129

790

791

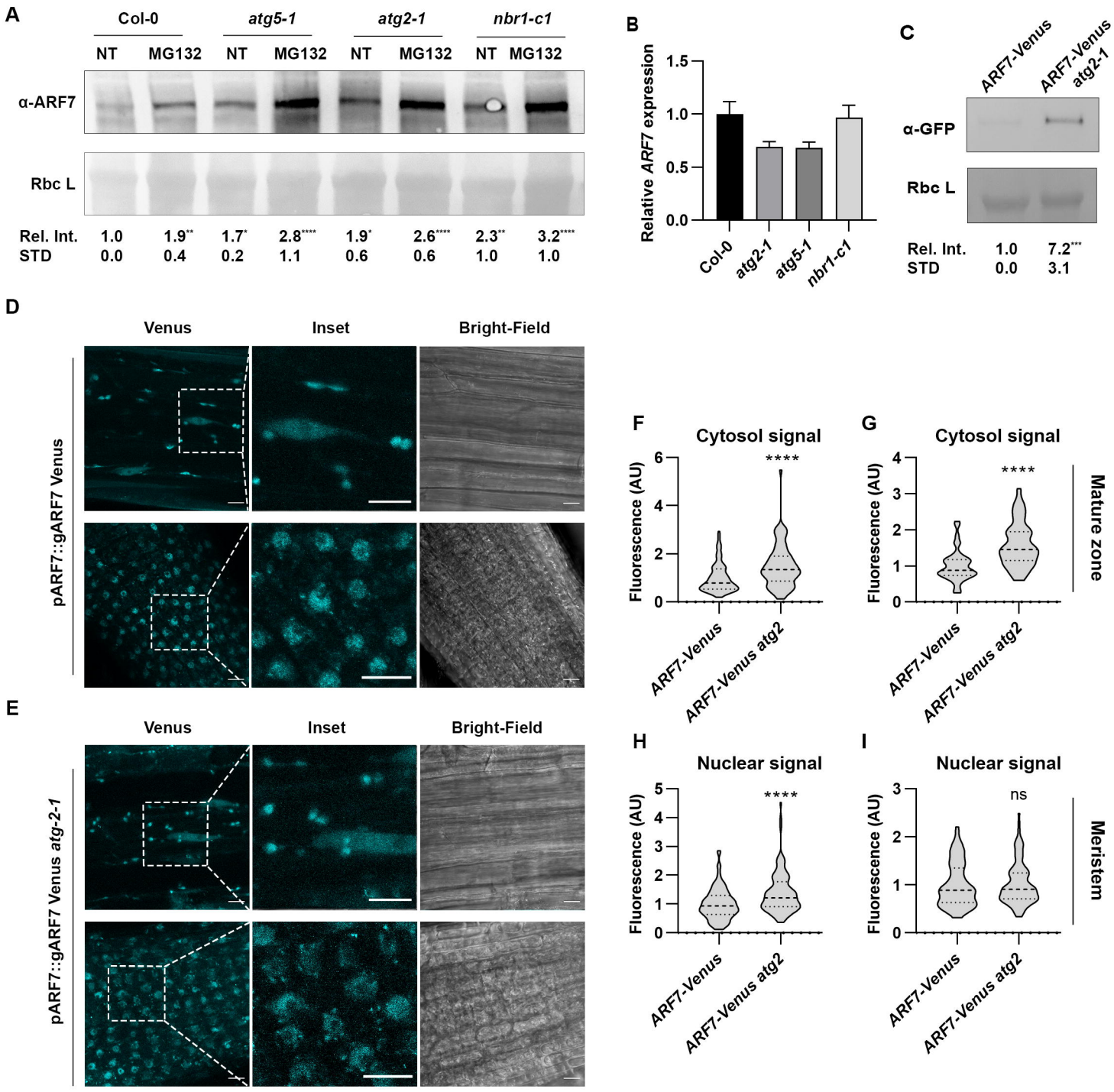
A
Col-0
atg5-1
atg2-1
nbr1-c1
NT
MG132
α-ARF7
Rbc L
Rel. Int. 1.0 1.9** 1.7* 2.8**** 1.9* 2.6**** 2.3** 3.2****
STD 0.0 0.4 0.2 1.1 0.6 0.6 1.0 1.0
B
Relative ARF7 expression
1.5
1.0
0.5
0.0
Col-0
atg2-1
atg5-1
nbr1-c1
C
ARF7-Venus
ARF7-Venus atg2-1
α-GFP
Rbc L
Rel. Int. 1.0 7.2***
STD 0.0 3.1
D
Venus
Inset
Bright-Field
pARF7::gARF7 Venus
E
Venus
Inset
Bright-Field
pARF7::gARF7 Venus atg-2-1
F
Cytosol signal
Fluorescence (AU)
****
ARF7-Venus
ARF7-Venus atg2
G
Cytosol signal
Fluorescence (AU)
****
Mature zone
ARF7-Venus
ARF7-Venus atg2
H
Nuclear signal
Fluorescence (AU)
****
ARF7-Venus
ARF7-Venus atg2
I
Nuclear signal
Fluorescence (AU)
ns
Meristem
ARF7-Venus
ARF7-Venus atg2

Figure 2

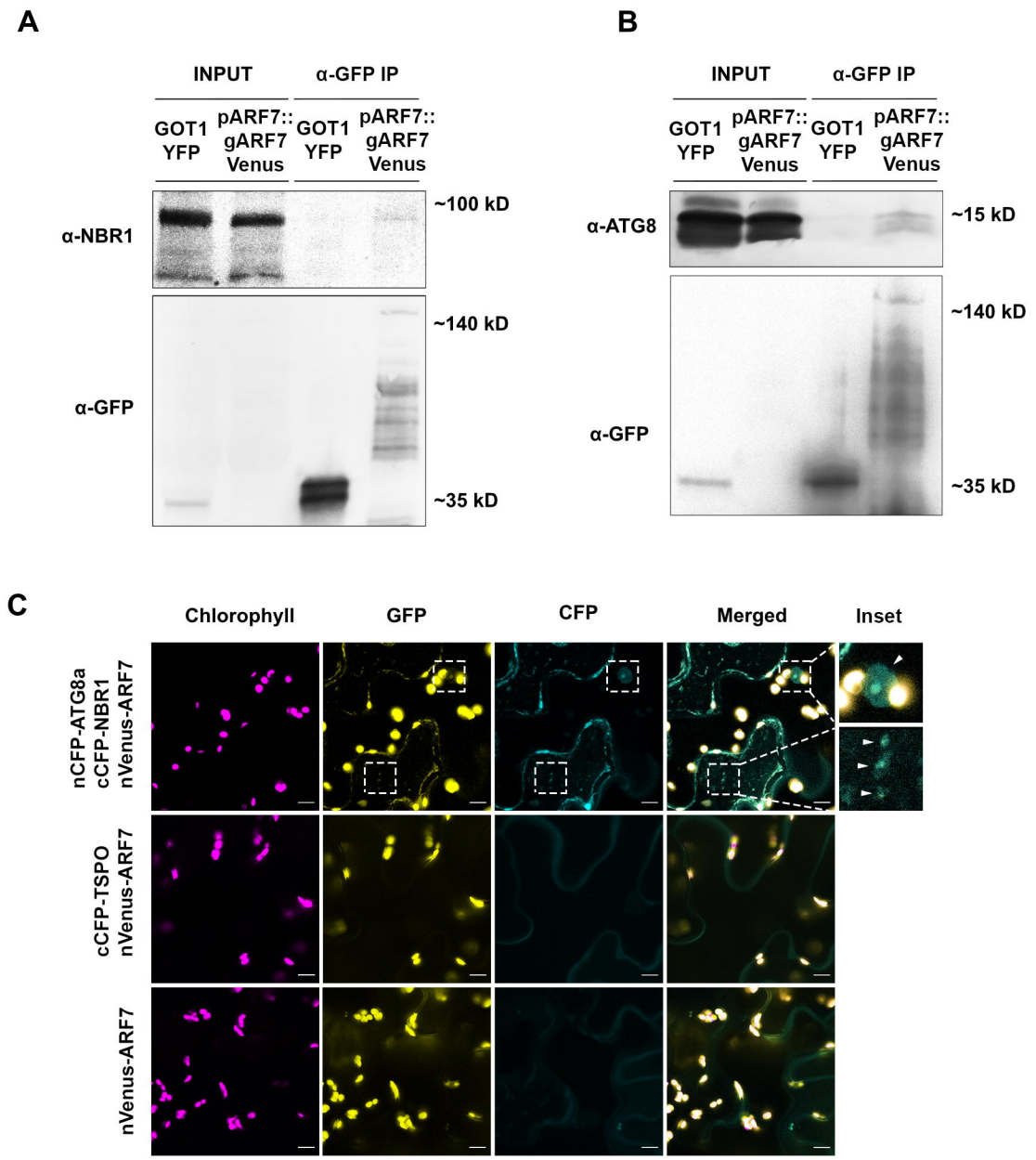
A
INPUT
α-GFP IP
GOT1 YFP
pARF7:: gARF7 Venus
GOT1 YFP
pARF7:: gARF7 Venus
α-NBR1
~100 kD
α-GFP
~140 kD
~35 kD
B
INPUT
α-GFP IP
GOT1 YFP
pARF7:: gARF7 Venus
GOT1 YFP
pARF7:: gARF7 Venus
α-ATG8
~15 kD
α-GFP
~140 kD
~35 kD
C
Chlorophyll
GFP
CFP
Merged
Inset
nCFP-ATG8a
cCFP-NBR1
nVenus-ARF7
cCFP-TSPO
nVenus-ARF7
nVenus-ARF7

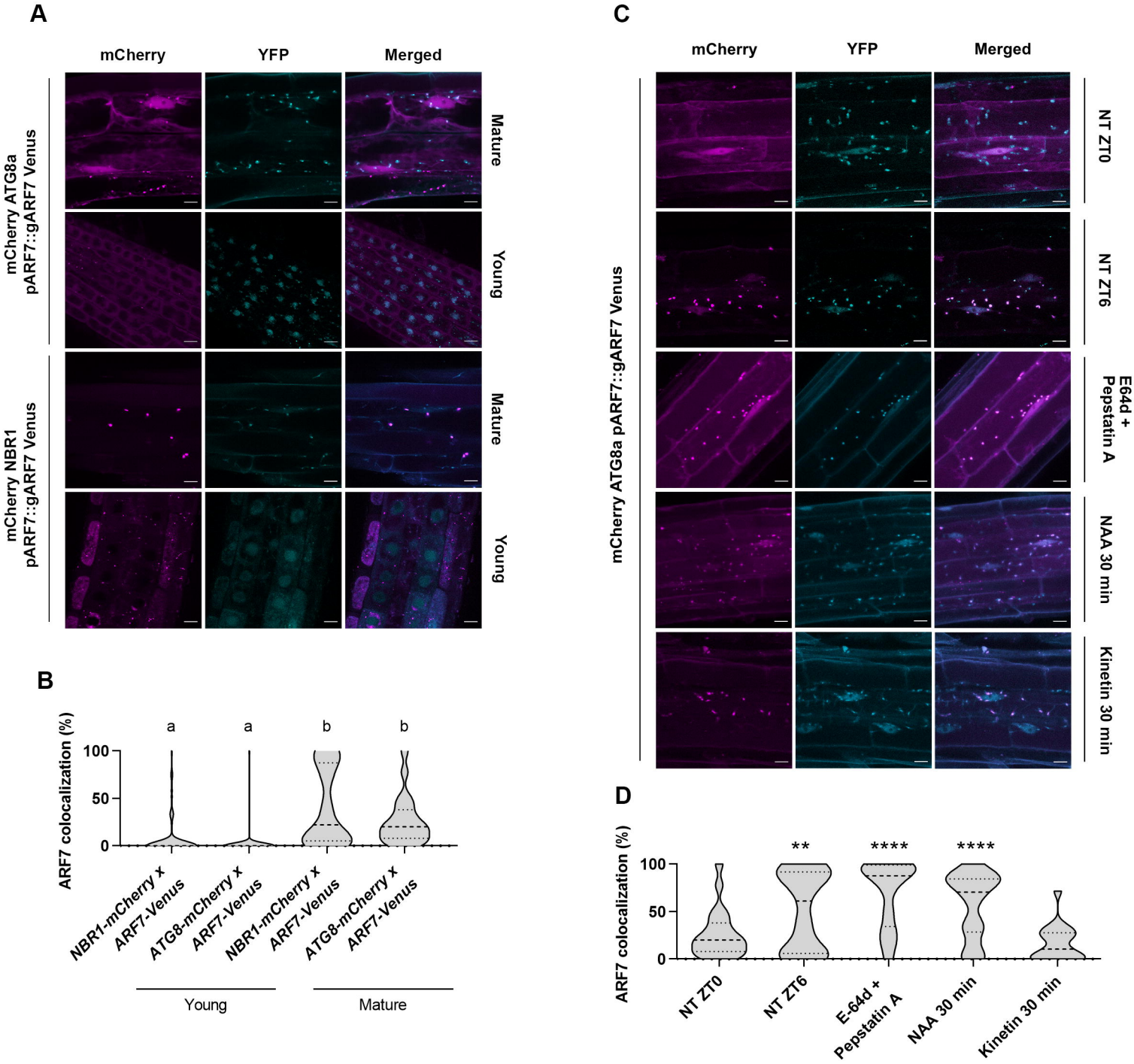
A
mCherry
YFP
Merged
mCherry ATG8a pARF7::gARF7 Venus
mCherry NBR1 pARF7::gARF7 Venus
Mature
Young
Mature
Young
B
ARF7 colocalization (%)
100
50
0
a
a
b
b
NBR1-mCherry x ARF7-Venus
ATG8-mCherry x ARF7-Venus
NBR1-mCherry x ARF7-Venus
ATG8-mCherry x ARF7-Venus
Young
Mature
C
mCherry
YFP
Merged
mCherry ATG8a pARF7::gARF7 Venus
NT ZT0
NT ZT6
E64d + Pepstatin A
NAA 30 min
Kinetin 30 min
D
ARF7 colocalization (%)
100
50
0
**
****
****
NT ZT0
NT ZT6
E-64d + Pepstatin A
NAA 30 min
Kinetin 30 min

Figure 4

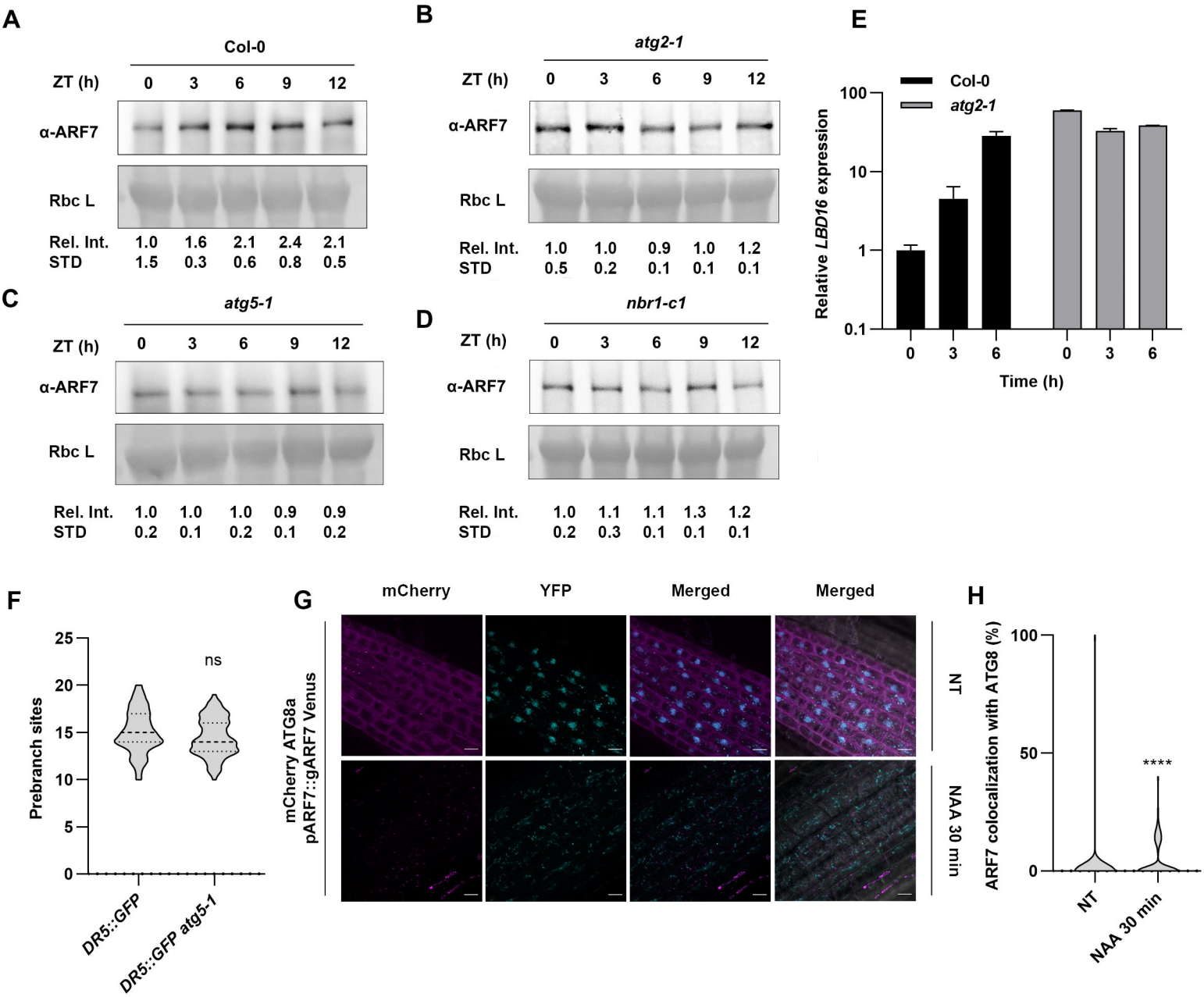
A
Col-0
ZT (h) 0 3 6 9 12
α-ARF7
Rbc L
Rel. Int. 1.0 1.6 2.1 2.4 2.1
STD 1.5 0.3 0.6 0.8 0.5
B
atg2-1
ZT (h) 0 3 6 9 12
α-ARF7
Rbc L
Rel. Int. 1.0 1.0 0.9 1.0 1.2
STD 0.5 0.2 0.1 0.1 0.1
C
atg5-1
ZT (h) 0 3 6 9 12
α-ARF7
Rbc L
Rel. Int. 1.0 1.0 1.0 0.9 0.9
STD 0.2 0.1 0.2 0.1 0.2
D
nbr1-c1
ZT (h) 0 3 6 9 12
α-ARF7
Rbc L
Rel. Int. 1.0 1.1 1.1 1.3 1.2
STD 0.2 0.3 0.1 0.1 0.1
E
Col-0
atg2-1
Relative LBD16 expression
100
10
1
0.1
0 3 6 0 3 6
Time (h)
F
Prebranch sites
25
20
15
10
5
0
ns
DR5::GFP
DR5::GFP atg5-1
G
mCherry
YFP
Merged
Merged
mCherry ATG8a
pARF7::gARF7 Venus
NT
NAA 30 min
H
ARF7 colocalization with ATG8 (%)
100
50
0
****
NT
NAA 30 min

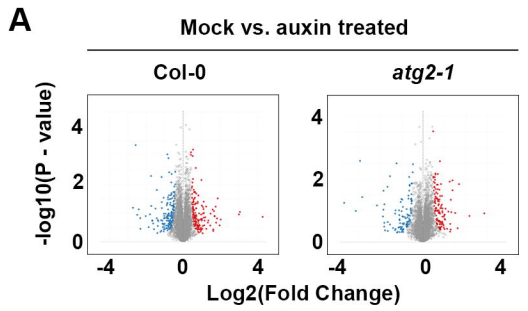
A
Mock vs. auxin treated
Col-0
atg2-1
-log10(P - value)
4
2
0
-4
0
4
Log2(Fold Change)

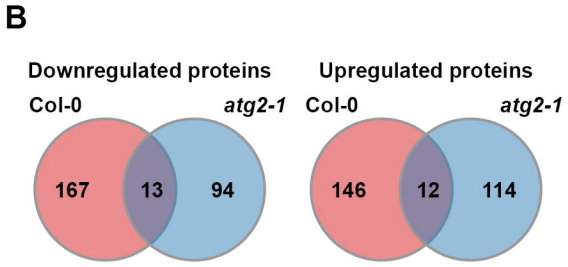
B
Downregulated proteins
Col-0
atg2-1
167
13
94
Upregulated proteins
Col-0
atg2-1
146
12
114

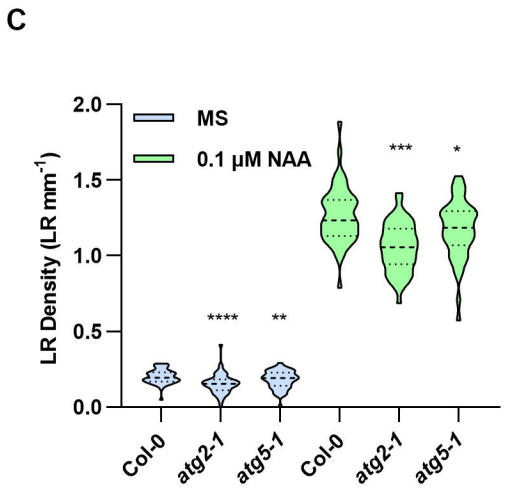
C
MS
0.1 μM NAA
LR Density (LR mm-1)
2.0
1.5
1.0
0.5
0.0
****
**
***
*
Col-0
atg2-1
atg5-1
Col-0
atg2-1
atg5-1

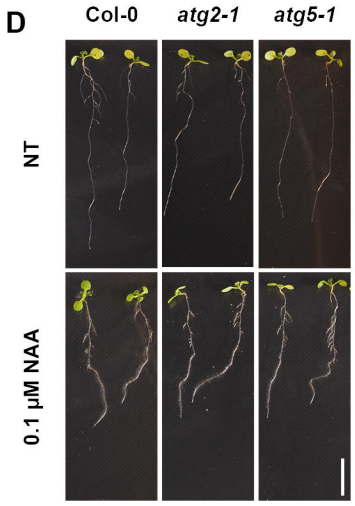
D
Col-0
atg2-1
atg5-1
NT
0.1 μM NAA